Check for updates

FIBROSIS

Copyright © 2024 The Authors, some rights reserved; exclusive licensee American Association for the Advancement of Science. No claim to original U.S. Government Works

An antibody that inhibits TGF-β1 release from latent extracellular matrix complexes attenuates the progression of renal fibrosis

Justin W. Jackson[1]†, Frederick C. Streich Jr.[1]†, Ajai Pal[1], George Coricor[1]‡, Chris Boston[1], Christopher T. Brueckner[1]§, Kaleigh Canonico[1], Christopher Chapron[1], Shaun Cote[1], Kevin B. Dagbay[1]¶, Francis T. Danehy Jr.[1], Mania Kavosi[1], Sandeep Kumar[1]#, Susan Lin[1], Christopher Littlefield[1]††, Kailyn Looby[1]‡‡, Rohan Manohar[1]††, Constance J. Martin[1]§§, Marcie Wood[1,2], Agatha Zawadzka[1], Stefan Wawersik[1]¶¶, Samantha B. Nicholls[1], Abhishek Datta[1]##, Alan Buckler[1], Thomas Schürpf[1]***, Gregory J. Carven[1]†††, Mohammed Qatanani[1], Adam I. Fogel[1]***

Inhibitors of the transforming growth factor–β (TGF-β) pathway are potentially promising antifibrotic therapies, but nonselective simultaneous inhibition of all three TGF-β homologs has safety liabilities. TGF-β1 is noncovalently bound to a latency-associated peptide that is, in turn, covalently bound to different presenting molecules within large latent complexes. The latent TGF-β–binding proteins (LTBPs) present TGF-β1 in the extracellular matrix, and TGF-β1 is presented on immune cells by two transmembrane proteins, glycoprotein A repetitions predominant (GARP) and leucine-rich repeat protein 33 (LRRC33). Here, we describe LTBP-49247, an antibody that selectively bound to and inhibited the activation of TGF-β1 presented by LTBPs but did not bind to TGF-β1 presented by GARP or LRRC33. Structural studies demonstrated that LTBP-49247 recognized an epitope on LTBP-presented TGF-β1 that is not accessible on GARP- or LRRC33-presented TGF-β1, explaining the antibody's selectivity for LTBP-complexed TGF-β1. In two rodent models of kidney fibrosis of different etiologies, LTBP-49247 attenuated fibrotic progression, indicating the central role of LTBP-presented TGF-β1 in renal fibrosis. In mice, LTBP-49247 did not have the toxic effects associated with less selective TGF-β inhibitors. These results establish the feasibility of selectively targeting LTBP-bound TGF-β1 as an approach for treating fibrosis.

INTRODUCTION

Organ fibrosis contributes to poor prognosis in many diseases, including chronic kidney disease, nonalcoholic steatohepatitis, and idiopathic pulmonary fibrosis. Even with this considerable unmet medical need, directly targeting the progression of fibrosis has proven challenging (*1*, *2*). Among the core molecular mechanisms driving fibrosis, the transforming growth factor–β (TGF-β) pathway is perhaps the most well established (*3*). Numerous preclinical studies have demonstrated the potential efficacy of TGF-β–directed approaches in lung, liver, and kidney fibrosis (*4*, *5*).

Despite this understanding, safely targeting the TGF-β pathway has proven challenging. Three TGF-β growth factors (GFs), TGF-β1, TGF-β2, and TGF-β3, are expressed by mammals and signal through similar receptor complexes that lead to activation of the activin receptor–like kinase 5 (ALK5) (*6*). Targeting all three GFs simultaneously with an antibody (*7*) or targeting the shared receptor with a kinase inhibitor (*8*) resulted in severe cardiac valvulopathies in rodent and primate models that necessitated modified dosing regimens in the clinic (*9*) and limited further development for therapeutic use in humans. Nonetheless, the potential for targeting the TGF-β pathway remains, with next-generation therapies focusing on more selective strategies to limit safety concerns.

Although the exact cause of the cardiac toxicities remains unclear, current evidence suggests that the inhibition of TGF-β1 signaling is not involved. Genetic studies in *Tgfb2* and *Tgfb3* knockout (KO) mice (*10*, *11*) have revealed developmental cardiac phenotypes, indicating that inhibition of TGF-β2 and TGF-β3, either alone or in combination, contributes to the issues seen with pharmacological agents targeting all three homologs. This is further supported by partial loss-of-function mutations in human patients described for both the *TGFB2* and *TGFB3* genes in genetically driven connective tissue disorders such as Marfan (*12*) and Loeys-Dietz (*13*) syndromes. Furthermore, we previously demonstrated that targeting TGF-β1 alone is a well-tolerated approach in preclinical safety studies, even with very high doses of a TGF-β1–specific monoclonal antibody (*14*). On the basis of this preclinical safety profile and evidence of a synergistic

[1]Scholar Rock Inc., 301 Binney Street, Cambridge, MA 02142, USA. [2]ToxStrategies LLC, 23501 Cinco Ranch Boulevard, Katy, TX 77494, USA.
*Corresponding author. Email: afogel@scholarrock.com
†These authors contributed equally to this work.
‡Present address: Shasqi Inc., 665 3rd Street, San Francisco, CA 94107, USA.
§Present address: Bristol-Myers Squibb, 250 Water Street, Cambridge, MA 02141, USA.
¶Present address: Keros Therapeutics, 1050 Waltham Street, Suite 302, Lexington, MA 02421, USA.
#Present address: DEM Biopharma, 730 Main Street, 5th Floor, Cambridge, MA 02139, USA.
**Present address: Radiant Therapuetics, 686 Bay Street, Toronto, ON M5G 0A4, Canada.
††Present address: Mediar Therapeutics, 20 Overland Street, Boston, MA 02215, USA.
‡‡Present address: Dyno Therapeutics, 343 Arsenal Street, Suite 101, Watertown, MA 02472,USA.
§§Present address: Generation Bio, 301 Binney Street, Cambridge, MA 02142, USA.
¶¶Present address: Q32 Bio, 830 Winter St., Waltham, MA 02451, USA.
##Present address: Scion Innovations, 134 Coolidge Avenue, #2, Watertown, MA 02472, USA.
***Present address: Incendia Therapeutics Inc., 40 Guest St., Boston, MA 02135, USA.
†††Present address: Curie.Bio, 68 Harrison Avenue #605, PMB 40851, Boston, MA 02111, USA.

Downloaded from https://www.science.org at Dalian University of Technology on November 13, 2025

effect with checkpoint blockade in preclinical models (*15*), a phase 1 trial in cancer immunotherapy was initiated with the TGF-β1–specific inhibitor SRK-181 (NCT04291079).

TGF-β1 is a pleiotropic signaling molecule with multiple effects in immune regulation, wound healing, and fibrosis. Despite the potential utility of inhibiting both immune cell–and extracellular matrix (ECM)–associated TGF-β1 in oncology, chronic targeting of TGF-β1 in organ fibrosis may benefit from a more selective approach. Immune cell activation, a key feature of the immunotherapy approach for TGF-β1 inhibition (*15*), may be undesirable in settings of chronic administration of an antifibrotic therapy. It has been demonstrated in renal fibrosis that regulatory T cells (T_{reg} cells) may protect the kidney from additional injury (*16*), suggesting that suppressing these cells through broad inhibition of TGF-β1 may be undesirable. Specifically targeting the profibrotic effects of TGF-β1 while sparing immune cell modulation would represent an attractive, targeted approach for a TGF-β1–directed antifibrotic intervention.

Achieving such a profile is possible by targeting TGF-β1 in its latent form in the context of its larger protein complex. TGF-β1 is not secreted in an active form by cells; instead, it is presented as a latent complex composed of the latency-associated peptide (LAP) and growth factor (GF), which are both part of the translated TGF-β1 protein and remain noncovalently associated with one another after furin cleavage in the Golgi apparatus (*17*). After secretion, this latent form of TGF-β1 requires integrin- or protease-mediated activation to release the GF and enable signaling through the TGF-β receptors (Fig. 1A) (*18*). The complex of the LAP and GF is referred to as latent TGF-β1 or the small latent complex (SLC). In vivo, the LAP is linked through disulfide bonds to proteins in the ECM, or transmembrane proteins, forming large latent complexes (LLCs). These LLC-forming proteins, or presenting molecules, include the latent TGF-β–binding proteins 1 and 3, (LTBP1 and LTBP3), both of which are ECM proteins that are themselves cross-linked to other ECM components (Fig. 1B) (*19*). By contrast, within the immune compartment, latent TGF-β1 is found bound to glycoprotein A repetitions predominant [GARP; also known as leucine-rich repeat–containing (LRRC) protein 32 (LRRC32)] on the surface of activated T_{reg} cells (Fig. 1C) (*20*) and to LRRC33 [also known as negative regulator of reactive oxygen species (NRROS)] on the surface of myeloid cells (Fig. 1D) (*21*). Because the macromolecular structure of LTBP-bound complexes of TGF-β1 differs considerably from that of the GARP- and LRRC33-bound TGF-β1 (*22–24*), we sought to identify antibodies selective for the LTBP-bound subsets of latent TGF-β1.

Here, we describe the characterization of LTBP-49247, a fully human monoclonal antibody that selectively inhibits the activation of LTBP-presented TGF-β1 while avoiding inhibition of GARP- and LRRC33-presented TGF-β1. LTBP-49247 bound to LLCs of TGF-β1 with LTBP1 or LTBP3, but not to GARP or LRRC33 complexes in vitro, and did not bind to TGF-β1 presented on T_{reg} cells by GARP. Structural studies revealed an epitope on latent TGF-β1 that provides the mechanistic basis for allosteric inhibition of TGF-β1 activation while simultaneously providing a hypothesis as to the inability of LTBP-49247 to bind GARP and LRRC33 complexes of TGF-β1. In two independent in vivo models of renal fibrosis, LTBP-49247 demonstrated antifibrotic efficacy comparable to that of a context-independent TGF-β1 inhibitor (an antibody that inhibits all four LLCs of TGF-β1), supporting the hypothesis that LTBP-presented TGF-β1 is the critical presentation context for profibrotic TGF-β1 in the kidney. In a 13-week preclinical mouse toxicology study, LTBP-49247 exhibited none of the toxicities seen with other TGF-β–targeting approaches. These results suggest that selectively targeting LTBP-presented TGF-β1 may be a promising avenue for

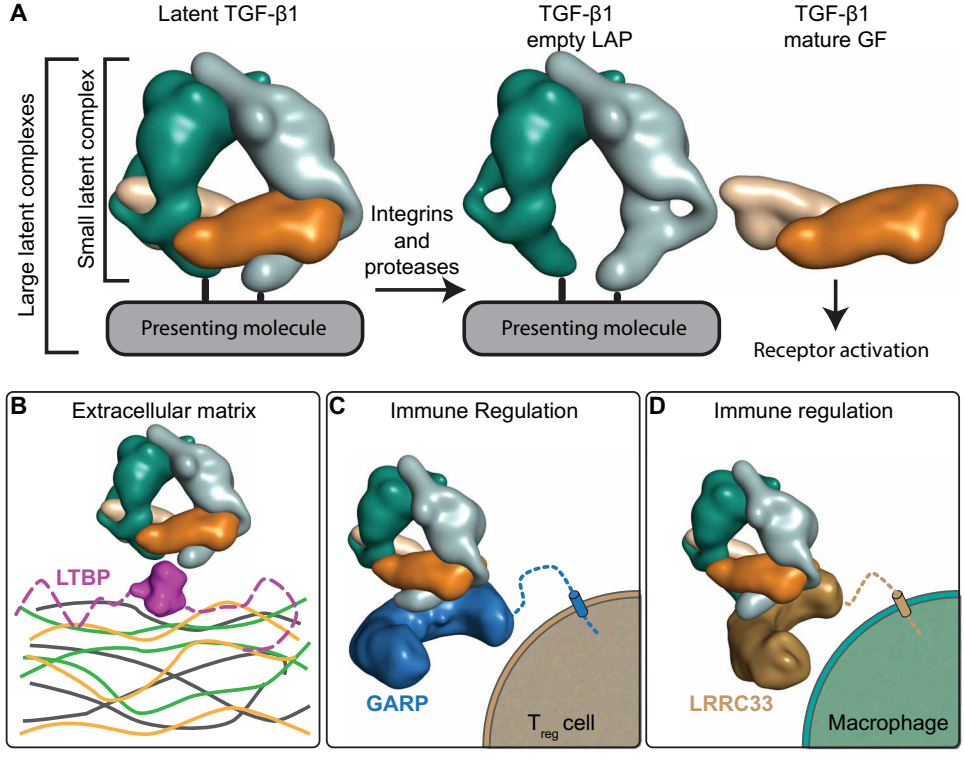

Fig. 1. TGF-β1 exists in different contexts as an inactive latent complex poised for activation, growth factor release, and signaling. (**A**) TGF-β1 exists in an inactive, dimeric form within latent complexes. The GF portion of TGF-β1 (orange and peach) is secreted in a small latent complex with LAPs (teal and blue) that become covalently linked to one of various potential presenting molecules, together constituting the large latent complexes. Upon activation by integrins or proteases, the mature GF is released from the LAP for receptor binding and signaling. (**B** to **D**) TGF-β1–LAP can bind to LTBP1 or LTBP3, forming complexes that become embedded into the extracellular matrix, a context relevant to fibrosis (B), or bind to GARP (C) or LRRC33 (D), forming complexes on cell surfaces in contexts relevant to immune regulation. Diagram created with PyMOL from PDBs 1KSQ, 6GFF, and 7Y1R (*22–24*).

Downloaded from https://www.science.org at Dalian University of Technology on November 13, 2025

the treatment of fibrosis while minimizing the risks associated with broadly targeting the TGF-β pathway.

RESULTS

LTBP-49247 selectively binds to LTBP-presented TGF-β1

A panel of antibodies selective for LTBP–TGF-β1 was found through multiple antibody display campaigns using human-derived naïve antibody libraries presented on the surface of either yeast or phage, as previously described (*15*). Selectivity for LTBP–TGF-β1 was achieved through a yeast display affinity maturation campaign involving mutagenesis of all complementarity-determining regions (CDRs) and subsequent positive selections for binding to LTBP-complexed TGF-β1 and negative selections against both free LTBP and the GARP–TGF-β1 complex (fig. S1). Hits were selected on the basis of affinity and binding selectivity for LTBP complexes of TGF-β1. Further screening was performed by evaluating inhibition of integrin-mediated activation of TGF-β1 in a cell-based assay described below. LTBP-49247 was selected as the lead LTBP complex–dependent inhibitory antibody. TGFb1-37021 is a context-independent antibody targeting latent TGF-β1 that was found through a similar process of in vitro display using human-derived naïve antibody libraries, followed by affinity maturation, but positive selections were performed with both LTBP and immune complexes of TGF-β1, and negative selections were performed with presenting molecules alone and complexes of TGF-β3.

Biolayer interferometry was used to evaluate the specificity of LTBP-49247 for latent TGF-β1. The TGF-β1 SLC (the GF plus LAP) or the mature GF forms of TGF-β1, TGF-β2, and TGF-β3 were coupled to biosensors using amine reactive tips, and LTBP-49247 binding was evaluated. LTBP-49247 exhibited robust binding only to the SLC of TGF-β1, with no binding observed to the mature GFs, indicating that the LAP is required for antibody binding (Fig. 2A). Next, LTBP-49247 was immobilized to the surface of anti-human Fc sensor tips, and binding of LTBP1–TGF-β1, LTBP1–TGF-β2, LTBP1–TGF-β3, and LTBP1 alone was tested. Robust binding was observed only to LTBP1–TGF-β1, indicating that LTBP-49247 is TGF-β1–selective (Fig. 2B).

We next used surface plasmon resonance (SPR) to further characterize the binding affinity of LTBP-49247 to the human TGF-β1 SLC and TGF-β1 LLCs, with TGFb1-37021 included as a comparator. Biotinylated SLC and LLCs were immobilized on the surface of a biotin CAPture sensor chip, and a titration of the antigen-binding fragments (Fabs) of each of the test antibodies was flowed over the prepared surface. LTBP-49247 Fab bound to the LTBP1 and LTBP3 complexes of TGF-β1 with subnanomolar affinity, bound the SLC with double-digit nanomolar affinity, and demonstrated minimal binding to either GARP–TGF-β1 or LRRC33–TGF-β1 (Fig. 2C). TGFb1-37021 Fab bound with subnanomolar affinity to the SLC and all four TGF-β1 LLCs.

To validate the selectivity of LTBP-49247 with an additional orthogonal method, a Meso Scale Discovery solution equilibrium titration (MSD-SET) (*25*) assay was performed to measure antibody binding to human, mouse, rat, and cynomolgus monkey TGF-β1 LLCs. LTBP-49247 bound with picomolar affinity to LTBP1–TGF-β1 and LTBP3–TGF-β1 with no binding to GARP–TGF-β1 or LRRC33–TGF-β1 (Fig. 2D and fig. S2, A to D) across all species tested, consistent with the robust binding observed using SPR. The high binding affinity, selectivity, and species cross-reactivity of LTBP-49247 support its use in the rodent models described below.

LTBP-49247 does not bind human T_{reg} cells

We next asked whether LTBP-49247 can interact with immune cells known to produce latent TGF-β1. Activated natural human T_{reg} cells produce GARP–TGF-β1, and TGF-β1 is an important signaling molecule in transmitting the immunosuppressive function of these cells (*20*, *26*). T_{reg} cells, defined as the $CD4^{+}CD25^{high}CD127^{low}$ population, were isolated from peripheral mononuclear cells by fluorescence-activated cell sorting and cultured for 4 days in the presence of plate-bound anti-CD3 (10 μg/ml) and soluble anti-CD28 (10 μg/ml) to induce activation. Cells were stained for CD4 and labeled with the test antibodies TGFb1-37021 and LTBP-49247, immunoglobulin G4 (IgG4) isotype control, or MHGARP8, which is an antibody that binds specifically to human GARP–TGF-β1 (*26*) and subjected to flow cytometry. MHGARP8 bound to 10.7% of the activated T_{reg} cells, and TGFb1-37021 bound 27.8% of activated T_{reg} cells (Fig. 2E), validating the presence of both GARP and TGF-β1 on the surface of these T_{reg} cells. The difference in apparent percent positivity between MHGARP8 and TGFb1-37021 may be due to affinity, stoichiometric, or target epitope availability differences between the two antibodies because both are able to bind to GARP–TGF-β1 complexes. By comparison, LTBP-49247 demonstrated less than 2% positivity, similar to that of the IgG4 isotype control (Fig. 2F). These results extend the selectivity profile of LTBP-49247 to a cellular context and demonstrate minimal interaction with a critical immune cell population producing latent TGF-β1.

LTBP-49247 inhibits integrin- and protease-mediated activation of TGF-β1

Given the lack of binding to GARP-presented TGF-β1 on activated T_{reg} cells, we next tested whether LTBP-49247 could inhibit TGF-β1 activation in the context of cellular assays in which LTBP presents TGF-β1. We first used LN229 cells, a human glioblastoma–derived cell line that has high expression of *LTBP3* without detectable expression of *LRRC32* (which encodes GARP) or *LRRC33* (fig. S3A) (*15*). This cell line produces high amounts of β_8 integrin, forming the integrin heterodimer $\alpha_v\beta_8$, which can activate TGF-β1 by binding to the arginine–glycine–aspartic acid (RGD) motif in the LAP (*27*, *28*). LN229 cells were transfected with a construct encoding TGF-β1, allowed to produce the SLC for 24 hours, and then incubated with LTBP-49247 or TGFb1-37021. Cells with a luciferase gene driven by 12 repeats of a cytosine-adenine-guanine-adenine (CAGA12) promoter were then used as a reporter of TGF-β signaling (*15*). Both LTBP-49247 and TGFb1-37021 caused a potent, concentration-responsive suppression of TGF-β–driven luciferase signal (Fig. 3A), indicating that LTBP-49247 blocks signaling of LTBP–TGF-β1 in a cell-based assay. The pan–TGF-β GF antibody 1D11 (*29*) served as a positive control in this assay. LTBP-49247 Fab and TGFb1-37021 Fab also each caused a potent concentration-responsive inhibition of LTBP–TGF-β1 in the same assay (fig. S3B), indicating that bivalent binding is not required for inhibitory activity. Neither LTBP-49247 nor TGFb1-37021 inhibited the signaling of latent TGF-β2 or latent TGF-β3 in the same assay, whereas the control antibody 1D11 retained activity, consistent with the specificity observed in the binding profile (fig. S3, C and D).

It is speculated that $\alpha_v\beta_8$ integrin activates TGF-β1 without requiring tensile force because β_8 integrin lacks a connection to the cytoskeleton that is made by other integrins, such as β_6 (*28*). To test whether the activity of LTBP-49247 and TGFb1-37021 extends to activation of TGF-β1 by other integrins, we used an SW480 cell line

Downloaded from https://www.science.org at Dalian University of Technology on November 13, 2025

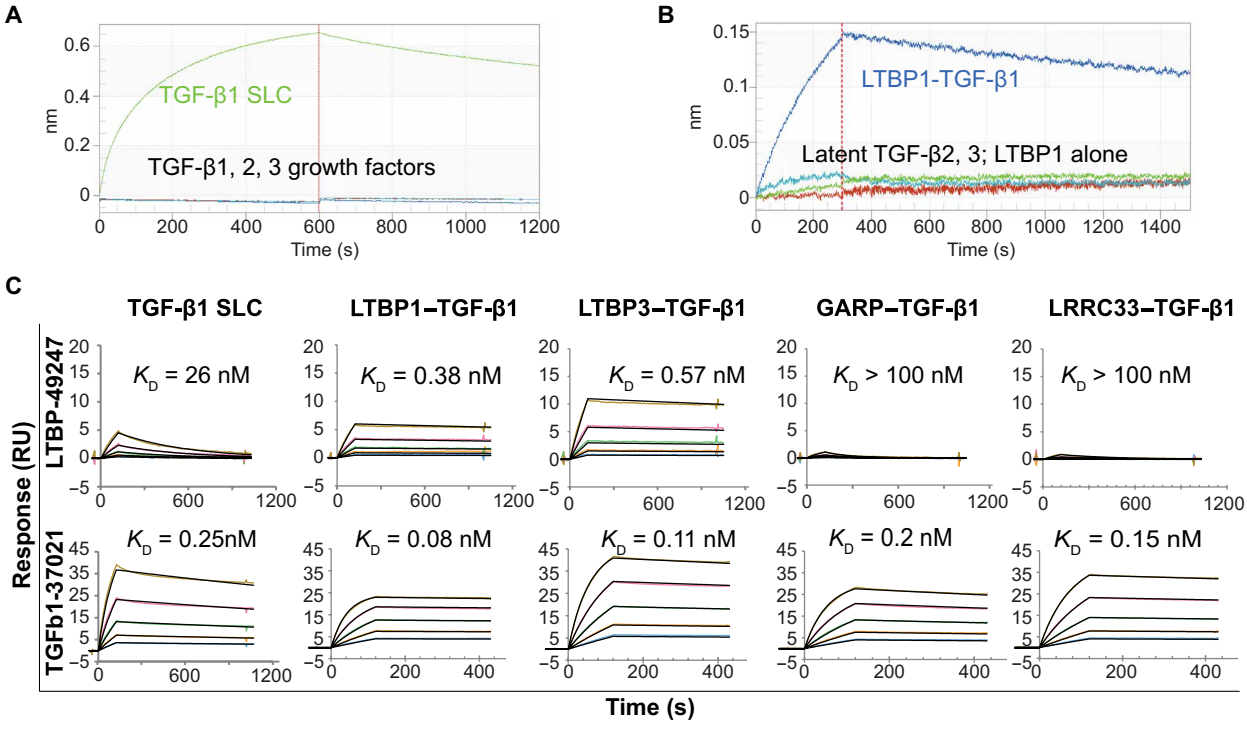

D MSD-SET affinities of LTBP-49247 to TGF-β1 complexes

Complex	Human	Mouse	Rat	Cyno
LTBP1–TGF-β1	40 pM	76 pM	8 pM	25 pM
LTBP3–TGF-β1	22 pM	9 pM	9 pM	27 pM
GARP–TGF-β1	n.b.	n.b.	n.b.	n.b.
LRRC33–TGF-β1	n.b.	n.b.	n.b.	n.b.

Fig. 2. LTBP-49247 binds specifically to TGF-β1 in latent complexes with LTBPs and does not bind to GARP or LRRC33 complexes. (**A**) LTBP-49247 binding to immobilized TGF-β1 SLC and to the mature growth factors TGF-β1, TGF-β2, and TGF-β3 was assessed by biolayer interferometry. Binding data are representative of three independent experiments. (**B**) LTBP-49247 binding to human LTBP1–TGF-β1, LTBP1–TGF-β2, and LTBP1–TGF-β3 was assessed by biolayer interferometry. Binding data are representative of three independent experiments. (**C**) Quantification of LTBP-49247 and TGFb1-37021 Fabs binding to biotinylated human SLC and large latent complexes of TGF-β1, as measured by surface plasmon resonance. Binding data are representative of three independent experiments. (**D**) LTBP-49247 binding to all known complexes of human, mouse, rat, and cynomolgus monkey TGF-β1 was measured using MSD-SET assays. Data are representative of two independent experiments, and the complete data are shown in fig. S2. n.b., no binding. (**E** and **F**) Equal concentrations of the antibodies MHGARP8, TGFb1-37021, LTBP-49247, and an isotype control were tested for binding to activated natural human T_{reg} cells by flow cytometry in separate stains (E), and percent positivity is graphed (F). Data are representative of two independent experiments.

Downloaded from https://www.science.org at Dalian University of Technology on November 13, 2025

with stable overexpression of β_6 integrin (SW480/b6 cells) because it is established that $\alpha_v\beta_6$ integrin activates TGF-β1 through the application of cytoskeleton-dependent mechanical force (*30*). Among the TGF-β1 presenting molecules, SW480/b6 cells produce only LTBP3 (fig. S3A). SW480/b6 cells were transfected with a construct encoding TGF-β1; allowed to produce the TGF-β1 SLC; and then incubated with STX-100, an $\alpha_v\beta_6$-blocking antibody (*31*), LTBP-49247 or TGFb1-37021, and CAGA12 reporter cells. STX-100 partially blocked TGF-β activity, indicating a predominant role for $\alpha_v\beta_6$ integrin in activation of TGF-β1 in this assay. As in the experiments in LN229 cells, LTBP-49247 and TGFb1-37021 caused a potent, concentration-responsive suppression of TGF-β signaling (Fig. 3B). These results indicate the capacity of LTBP-49247 and TGFb1-37021 to block integrin-mediated activation of TGF-β1 by multiple RGD-binding integrins.

We next tested whether LTBP-49247 can also inhibit protease-mediated activation of latent TGF-β1. Kallikrein, plasmin, and related proteases activate TGF-β1 by cleaving within the LAP, which causes dissociation of the GF and enables signaling (fig. S4, E and F) (*32*, *33*). In this assay, we added purified TGF-β1 SLC to CAGA12 luciferase reporter cells. In the absence of protease-mediated activation with kallikrein, there was little TGF-β1 signaling. In contrast, the addition of kallikrein drove considerable TGF-β1 signal, which was inhibited by either LTBP-49247 or TGFb1-37021, as well as the pan–TGF-β GF antibody 1D11, but not by isotype control (Fig. 3C). Although the blockade of kallikrein-mediated activation of TGF-β1 was definitive, the binding of LTBP-49247 or TGFb1-37021 did not prevent the proteolytic cleavage of the TGF-β1 SLC as assessed by SDS–polyacrylamide gel electrophoresis (PAGE) and Western blotting under denaturing conditions (Fig. 3D). This suggests that these antibodies may block signaling by preventing dissociation of the GF from the LAP. In combination, these data indicate that LTBP-49247 is capable of inhibiting both integrin- and protease-mediated activation of latent TGF-β1 in cell-based assays.

Structural data demonstrate the selectivity of LTBP-49247 for latent TGF-β1

The selectivity and inhibitory mechanism of LTBP-49247 prompted detailed structural studies to characterize the epitope and mechanism underlying the observed selectivity and inhibition. We therefore determined the crystal structure of the Fab portion of LTBP-49247 in complex with the TGF-β1 SLC, which was solved to a resolution of 2.21 Å (table S1). The crystal structure asymmetric unit features the TGF-β1 SLC (with a furin mutation to maintain a LAP-GF fusion for sample homogeneity) bound by two LTBP-49247 Fabs, one to each TGF-β1 protomer (Fig. 4A). The interaction of each Fab with TGF-β1

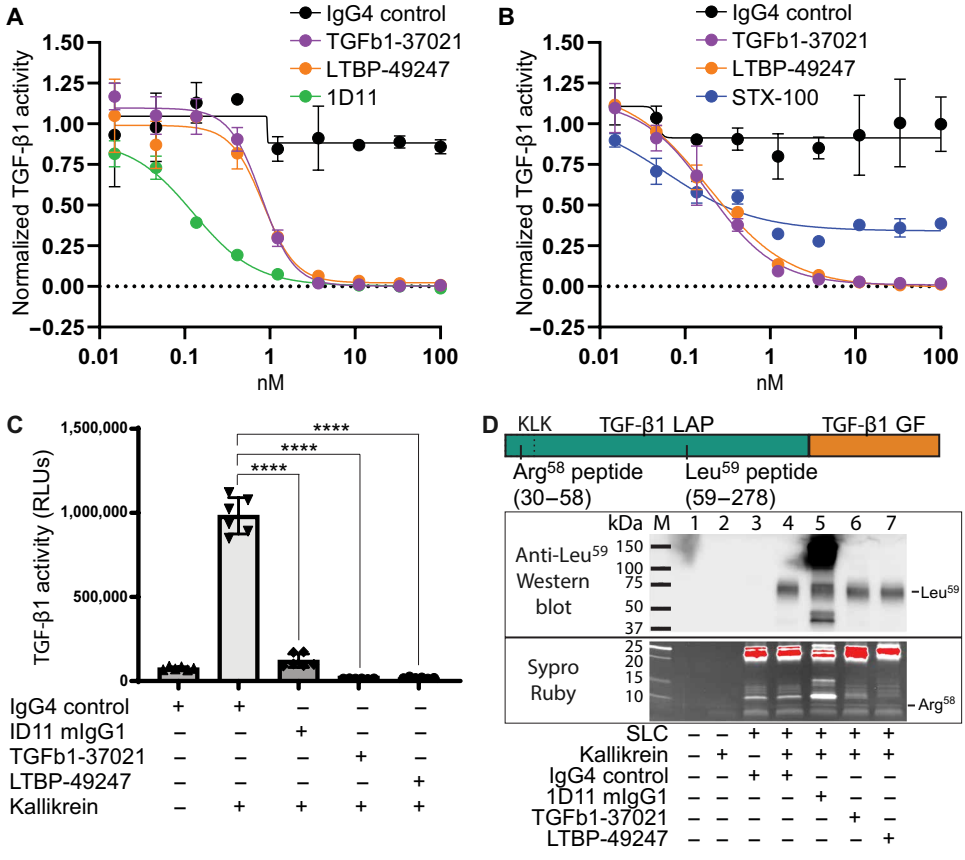

Fig. 3. LTBP-49247 inhibits integrin- and kallikrein-mediated activation of TGF-β1. (**A**) The effect of antibodies on integrin-mediated TGF-β1 activation was measured in a cell-based assay. Integrin $\alpha_v\beta_8$–expressing LN229 cells producing the TGF-β1 SLC were incubated with control IgG or serially diluted 1D11, LTBP-49247, or TGFb1-37021 and CAGA12 luciferase reporter cells. Data are shown normalized to antibody vehicle controls. The results are representative of three independent experiments. (**B**) SW480 cells stably expressing the integrin β_6 subunit (SW480/b6 cells) were transfected with a construct encoding TGF-β1 and treated with control IgG or STX-100, LTBP-49247, or TGFb1-37021 at the concentrations indicated, before addition of CAGA12 luciferase reporter cells. Data were normalized to antibody vehicle controls. The results are representative of three independent experiments. (**C**) The effect of antibodies was measured in a kallikrein-mediated TGF-β1 activation assay. CAGA12 luciferase reporter cells were cultured for 18 hours with TGF-β1 SLC, kallikrein, and the indicated antibodies before collection of luminescence data. RLUs, relative luciferase units. Results shown are the average of six replicates, and the experiment was performed two independent times with similar results. ****$P \leq 0.0001$, one-way analysis of variance (ANOVA) with comparison to IgG control + kallikrein. (**D**) The schematic illustrates the primary structure of the TGF-β1 GF in complex with the LAP and the location of the kallikrein (KLK) cleavage site between Arg^{58} and Leu^{59} in the LAP. Two SDS-PAGE gels were loaded with the identical samples of TGF- β1 SLC-antibody-kallikrein mixtures applied to the reporter cells in (C). One was blotted and probed with an antibody specific for the Leu^{59} peptide, and the other was stained with Sypro Ruby to show total proteins. The extra signal in lane 5 of the Western blot results from the recognition of the 1D11 mouse IgG1 antibody on the membrane by the secondary antibody. The location of the Arg^{58} peptide is noted on the Sypro Ruby–stained gel. The red color indicates saturated pixels. Images are representative of two independent experiments.

Downloaded from https://www.science.org at Dalian University of Technology on November 13, 2025

buries an average of 758 Å^2 of solvent-accessible surface on the TGF-β1 epitope. The Fab CDRs interact with the TGF-β1 LAP N-terminal α helix 1 (residues 36 to 47, UniProt numbering) and a finger domain of the of TGF-β1 GF (residues 299 to 305). This interaction is consistent with hydrogen deuterium exchange mass spectrometry (H/DX-MS) experiments (fig. S4, A to F). H/DX-MS is an extensively used structural characterization tool to probe higher-order structures of proteins including protein-protein or protein-ligand interactions (*34*). The bipartite binding of both the LAP and the GF likely speaks to the ability of LTBP-49247 to potently inhibit activation of TGF-β1 by stapling the LAP and the GF together and preventing their dissociation (Fig. 4B).

The LTBP-49247 Fab interactions with the LAP N-terminal α helix are mediated by residues on the CDR H1 (residues 26 to 33 by international ImMunoGeneTics information system numbering) and CDR H3 (residues 97 to 110) loops, whereas the role of the CDR H2 loop (residues 51 to 58) is primarily to bolster the conformation of the CDR H1 loop on the side away from the epitope (fig. S5, A to E, and table S2). The LTBP-49247 Fab interactions with the GF finger are mediated by residues on CDR H1 and all three light chain CDRs (residues 26 to 33, 51 to 55, and 92 to 101). The residues responsible for the interactions are summarized in table S2. Although the overall TGF-β1:LTBP-49247 Fab interface is very similar between the two epitope:paratope interface copies present in the structure, there are

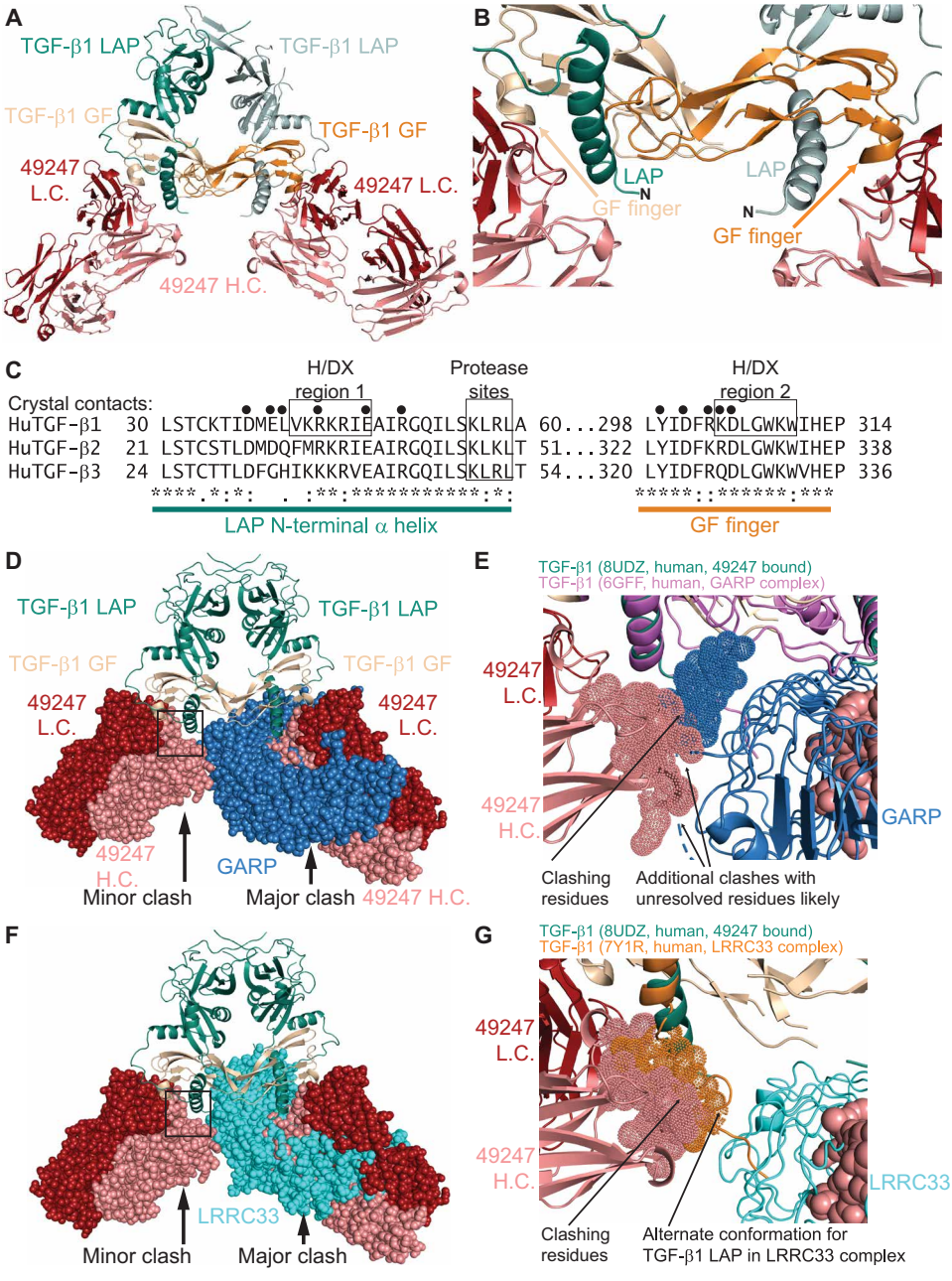

Fig. 4. Structure of the LTBP-49247 Fab bound to TGF-β1 small latent complex and insights into LTBP-49247's specificity. (**A**) Overview of the LTBP-49247 Fabs (L.C., light chain; H.C., heavy chain) bound to TGF-β1 GF and LAP in the SLC. (**B**) Zoom of the epitope:paratope interface and the interaction of the Fab with both the LAP and GF portions of the SLC. (**C**) Clustal omega alignment of the human TGF-β1, TGF-β2, and TGF-β3 sequences corresponding to the epitope on TGF-β1. Protected regions on TGF-β1 identified in H/DX-MS experiments are boxed, as is the site of protease cleavage for known activating proteases (kallikreins and plasmin). TGF-β1 epitope residues identified from the crystal structure are identified with black dots. The degree of conservation between the three homologs is annotated with symbols beneath the alignment: An asterisk (*) indicates positions that have a conserved residue; a colon (:) indicates conservation of residues with very similar properties; a period (.) indicates conservation of residues with weakly similar properties (*72*). (**D**) Alignment of two copies of a TGF-β1:LTBP-49247 Fab unit onto the TGF-β1 of the GARP- TGF-β1 structure (PDB: 6GFF), showing only the TGF-β1:LTBP-49247 Fab from the structure presented here and the GARP molecule. (**E**) Detailed view of the boxed area in (D), showing the TGF-β1 from both the structure presented here and the GARP structure. Clashing residues from GARP and the LTBP-49247 Fab heavy chain are shown with space-filling dots. (**F**) Alignment of two copies of a TGF-β1:49247 Fab unit onto the TGF-β1 in the LRRC33- TGF-β1 structure (PDB: 7Y1R), showing only the TGF-β1:LTBP-49247 Fab from the structure presented here and the LRRC33 molecule. (**G**) Detailed view of the boxed area in (F), showing the TGF-β1 from both the structure presented here and the LRRC33 structure. Clashing or incompatible residues from TGF-β1 (in the LRRC33 complex) and the LTBP-49247 Fab heavy chain are shown with space-filling dots.

Downloaded from https://www.science.org at Dalian University of Technology on November 13, 2025

minor residue conformation and interaction differences (fig. S5, B to E). At the chain B LAP:chain A GF interface, the contacts are more numerous than at the chain A LAP:chain B GF interface (fig. S5, B to E). The LTBP-49247 Fab interacts with residues on the LAP and GF that are unique between TGF-β1 and the other TGF-β homologs, which explains why it is specific for TGF-β1 and does not bind TGF-β2 or TGF-β3 (Figs. 2, A and B, and 4, A to C; and fig. S4, A to F). Notably, TGF-β1 residues Glu^{39}, Leu^{40}, Arg^{303}, and Lys^{304} are interaction residues that are unique to TGF-β1 and likely contribute to the observed specificity. Overall, these structural data explain the selectivity of LTBP-49247 for TGF-β1 as compared with TGF-β2 or TGF-β3.

LTBP-49247 binds to a structural epitope on LTBP–TGF-β1 but not GARP–or LRRC33–TGF-β1

We next sought a structural explanation for the selectivity of LTBP-49247 for LTBP-complexed TGF-β1 as compared with GARP- or LRRC33-complexed TGF-β1. The TGF-β1 LAP-GF in the structure presented here is found in a typical homodimer orientation with an overall conformation similar to that observed in previous SLC structures (fig. S6, A and B) (*18*, *30*, *35*). Two structures of human [Protein Data Bank (PDB): 5VQP] and porcine (PDB: 3RJR) TGF-β1 extend two more turns at the N terminus compared with the structure of integrin-bound human TGF-β1 (PDB: 5FFO) and the structure presented here for TGF-β1 in complex with the LTBP-49247 Fab (PDB: 8UDZ) (fig. S6, A and B). The structure presented here and 5FFO both have a slight "pinching in" of the N-terminal α helices. Because this slight conformational difference is observed in the absence of LTBP-49247, this conformation is likely not induced by LTBP-49247 Fab binding. Similarly, the TGF-β1 LAP-GF from the structure presented here aligns well with the global conformation of the TGF-β1 observed in the GARP (PDB: 6GFF) and LRRC33 (PDB: 7Y1R) complex structures except for some conformational differences at the N-terminal α helices (fig. S6, C and D) (*23*, *24*).

To model the positioning of the LTBP-49247 Fab on TGF-β1 presented in a GARP or LRRC33 complex, molecular alignments were created and interrogated for potential clashes or conformational incompatibilities. To create these alignments, one TGF-β1 LAP-GF:LTBP-49247 Fab complex unit was duplicated four times, and the TGF-β1 portion was aligned to each TGF-β1 protomer present in the GARP–TGF-β1 (PDB: 6GFF) or LRRC33–TGF-β1 (PDB: 7Y1R) complexes (fig. S6, C and D). Displaying GARP (Fig. 4, D and E) or LRRC33 (Fig. 4, F and G) illustrates that the way a TGF-β1 protomer with bound LTBP-49247 Fab would juxtapose with each presenting molecule. For both GARP and LRRC33, there is a major clash with the Fabs on the right and more subtle clash (GARP) or incompatibility (LRRC33) with the Fabs on the left (Fig. 4, D to G). In the case of GARP, the Fab on the left clashes with GARP residues that are present on a loop between two LRRs, which binds the underside of TGF-β1 (Fig. 4E). This clash is likely more pronounced than the model suggests because there are many residues from this loop that are disordered and not resolved in the structural model. In addition, it should be acknowledged that the GARP structure itself has a Fab bound to the TGF-β1:GARP interface and may stabilize or promote a particular conformation of the complex. In the case of LRRC33, the Fab on the left has no apparent clashes with LRRC33. However, the TGF-β1 N-terminal residues of the left protomer (part of the LTBP-49247 Fab epitope) adopt a conformation incompatible with LTBP-49247 binding (Fig. 4G). Note that for the LRRC33–TGF-β1 cryo–electron microscopy structure discussed above (PDB: 7Y1R), there were many apparent conformational bins, with nearly equal particle distribution across bins. The deposited complex model, used in the alignments here, derives from a subset of particles in one of these bins; thus, the model is a subset of conformations observed. In total, these data suggest that LTBP-49247 may specifically bind to LTBP complexes of TGF-β1 because of steric clashes or conformational incompatibility imposed by GARP and LRRC33 proximal to the TGF-β1 LAP in the LLCs (fig. S7, A to D).

LTBP-49247 reduces TGF-β signaling and fibrosis in a mouse model of Alport syndrome

TGF-β signaling is well established as a central driver of fibrosis across multiple organs. Kidney fibrosis presents a high unmet medical need and is therefore an important target for antifibrotic therapeutics. TGF-β1 is increased in the glomerular basement membrane in human kidney disease and correlates with the deposition of ECM components (*36*, *37*). Despite the importance of TGF-β1 to the progression of renal fibrosis, it may not be necessary or desirable to inhibit the TGF-β1 signaling component found in renal immune cells such as T_{reg} cells, which may serve a protective role in the longer-term progression of renal disease (*16*).

We evaluated LTBP-49247 in rodent models of kidney disease to test the hypothesis that inhibition of TGF-β1 signaling complexed with LTBP is sufficient to slow the progression of fibrosis. We first examined a genetic model of Alport syndrome, in which the gene encoding a critical glomerular basement membrane collagen, *Col4a3*, has been knocked out. Using an F1 cross of S129 and C57Bl/6 *Col4a3* heterozygous mice generated an intermediate phenotype between severe (*38*) and mild (*39*) models, consistent with the phenotype reported elsewhere (*40*). The resulting F1 homozygotes develop progressive kidney disease with mortality between 14 and 18 weeks of age.

LTBP-49247 allowed us to test whether the TGF-β1 signaling in the Alport model was driven to a substantial extent by LTBP–TGF-β1. We used *Col4a3* KO mice aged 11 weeks in a single-dose target engagement study (fig. S8A). We first evaluated TGF-β signaling by measuring changes in the number of nuclei positive for phosphorylated SMAD2 (pSMAD2), a transcriptional regulator that mediates cellular responses to TGF-βs, by immunohistochemistry and quantitative image analysis. Consistent with an increase in profibrotic TGF-β signaling and glomerulosclerosis, we observed a significant increase in the number of cells with pSMAD2^{+} nuclei in kidneys from homozygous (*Col14a3*$^{-/-}$) animals compared with heterozygote (*Col14a3*$^{+/-}$) littermates, particularly in the glomeruli themselves (fig. S8B). LTBP-49247 reduced the number of pSMAD2^{+} nuclei to the same extent as treatment with TGFb1-37021, which suppresses the activation of all latent TGF-β1 complexes, indicating that immune cell–associated TGF-β1 is not a major source of TGF-β1 signaling in this model of renal fibrosis. Consistent with the TGF-β pathway suppression observed by pSMAD2 quantification, LTBP-49247 and TGFb1-37021 also reduced the expression of the profibrotic genes *Col1a1* and *Mmp9* (fig. S8C). The similar effect of LTBP-49247 to TGFb1-37021 was not due to differences in antibody amounts because the concentrations of both antibodies in the serum were similar at the end of the study (fig. S8D).

The equivalent extent of target engagement for both LTBP-49247 and TGFb1-37021 suggested that the dominant source of disease-associated TGF-β1 in the Alport model was from LTBP-presented TGF-β1. Profiling of kidney tissue revealed that the expression of transcripts encoding all three TGF-β homologs, as well as all four presenting molecules, was increased in Alport KO kidneys compared

Downloaded from https://www.science.org at Dalian University of Technology on November 13, 2025

with those of heterozygous littermate controls (fig. S9). In combination with the activity of LTBP-49247, this result suggests that the predominant source of TGF-β signaling that drives fibrosis in this model is TGF-β1 presented by LTBP1 and/or LTBP3.

Given that a single dose of an antifibrotic agent is unlikely to substantially alter disease progression, we next evaluated the Alport model using twice weekly dosing over the course of a 6-week study (Fig. 5A). As with the single-dose study in the Alport model, both LTBP-49247 and TGFb1-37021 suppressed the number of $pSMAD2^+$ nuclei after 6 weeks of dosing (Fig. 5B). This end point suppression of TGF-β signaling combined with the sustained concentration in serum of the antibodies we observed in this model (fig. S10) suggests that there was consistent inhibition of TGF-β signaling. To evaluate the effect of this on fibrosis, we measured hydroxyproline (OH-P), a biochemical surrogate for total collagen quantity, in kidneys. We observed a significant reduction in OH-P content at all doses of LTBP-49247 examined, similar to the OH-P reduction observed with the antibody TGFb1-37021 that inhibits TGF-β1 regardless of the presenting molecule present (Fig. 5C). Consistent with this, *Col1a1* and *Col3a1* gene expression was also reduced with either LTBP-49247 or TGFb1-37021 treatment (Fig. 5D). To further confirm a reduction in fibrosis, we evaluated picrosirius red staining (PSR) using quantitative image analysis. Although the PSR data were more variable than the OH-P data, we observed a trend toward a reduction in PSR^+ area at higher doses of LTBP-49247 and TGFb1-37021 (Fig. 5E), suggesting a reduced progression of fibrosis with matrix-associated TGF-β1 inhibition.

LTBP-49247 reduces fibrotic progression in a rat model of chronic kidney disease

We evaluated a second model of kidney disease in which male Sprague-Dawley rats are fed a diet of 0.25% adenine. This causes the deposition of adenine crystals in the proximal tubules of the kidney, resulting in inflammation and interstitial fibrosis (*41*). The distinct nature of the insult allowed us to ask whether the role of LTBP-presented TGF-β1 signaling in the progression of fibrosis is applicable in different models of kidney fibrosis.

TGF-β pathway signaling in this model was first determined in a single-dose study. Disease was induced with 7 weeks of 0.25% adenine diet before a single dose of TGF-β–targeting antibody or the small-molecule ALK5 inhibitor (SB-525334) was administered to detect changes in TGF-β pathway signaling (fig. S11A). In contrast to our results in the single-dose Alport model study, we observed differential suppression of TGF-β signaling with the context-independent TGF-β1 inhibitor TGFb1-37021 compared with LTBP-49247 (fig. S11B) as evaluated by pSMAD2 quantification. High-dose TGFb1-37021 achieved a suppression of $pSMAD2^+$ nuclei close to the extent of reduction observed for the ALK5 inhibitor, which inhibits the shared receptor of TGF-β1, TGF-β2, and TGF-β3, indicating a predominance of TGF-β1 signaling among the homologs of TGF-β in this paradigm. However, LTBP-49247, even at high dose, showed minimal pathway suppression. The differences in TGF-β pathway suppression between LTBP-49247 and TGFb1-37021 were not due to differences in antibody concentrations in serum because these were similar between the two antibodies (fig. S11C). These differences may indicate a greater extent of immune cell TGF-β1 signaling in this model compared with the Alport model.

We next characterized the effect of the 0.25% adenine diet on the expression of TGF-β homologs and presenting molecules in the kidneys of these rats. The 0.25% adenine diet induced increased expression of the transcripts encoding all three TGF-β homologs, LTBP3, GARP, and LRRC33 (fig. S12). The induction of *Ltbp1* expression was minimal, and the induction of *Ltbp3* was moderate, suggesting that there is lower overall LTBP production in this model compared with the Alport model. This is consistent with the minimal reduction of pSMAD2 activation with LTBP-49247 as compared with TGFb1-37021.

Despite the apparent predominance of immune-associated TGF-β1 signaling as assessed by measuring $pSMAD2^+$ nuclei, we next asked whether LTBP-49247 might be sufficient to drive an antifibrotic effect in the rat adenine model. After 2 weeks on the adenine diet, dosing was initiated with antibody given twice weekly or ALK5 inhibitor given twice daily for the remaining 6 weeks (Fig. 6A). We used a loading dose for our antibodies in this multidose study to maintain stable concentration of antibodies in serum through the study. Consistent with our single-dose TGF-β pathway suppression study in this model, TGFb1-37021 exhibited significant reduction of $pSMAD2^+$ nuclei at high dose, whereas LTBP-49247 did not (Fig. 6B). Because of this difference between the two antibodies, we further examined the role of pSMAD2 signaling in subsets of cells using multiplexed fluorescent immunohistochemistry to identify cells positive for CD31 or CD45, which are standard markers for endothelial cells, which express GARP, and leukocyte cell populations, which can express either LRRC33 or GARP, respectively. Comparing the high dose of LTBP-49247 with the high dose of TGFb1-37021, we observed a strong repression of pSMAD2 in both endothelial and leukocyte populations with TGFb1-37021, whereas LTBP-49247 did not have activity on these cells (fig. S13A). These results are consistent with the lack of binding of LTBP-49247 to GARP- or LRRC33–TGF-β1 complexes on immune cells, supporting selectivity in vivo for LTBP-49247, at least in the context of the adenine diet model of kidney disease.

We next examined the degree of fibrosis at study end using biochemical measurement of OH-P. The data demonstrated a significant reduction in fibrosis with either LTBP-49247 or TGFb1-37021, which was equivalent for both doses tested (Fig. 6C). To further confirm the observed changes in fibrosis, we measured PSR by quantitative image analysis. The reduction in PSR^+ area was in agreement with the reductions in OH-P for both LTBP-49247 and TGFb1-37021, further indicating a reduction in fibrosis with specific inhibition of matrix-associated TGF-β1 in addition to context-independent TGF-β1 inhibition (Fig. 6D). Concentration of the antibodies in serum measured over time in this study were similar for LTBP-49247 and TGFb1-37021 (fig. S13B), ruling out the possibility that differences in pSMAD2 and fibrosis were due to different amounts of antibody over the course of the study. In combination with the selective modulation of pSMAD2 observed in this model, these data indicate that LTBP-49247 reduces the progression of renal fibrosis without substantially modulating TGF-β signaling on endothelial or immune cells. Furthermore, they demonstrate the broader ability of selective inhibition of LTBP–TGF-β1 to modulate renal fibrosis independent of etiology.

LTBP-49247 demonstrates no toxicities in a 13-week study in mice

With the confirmation of target engagement and antifibrotic activity for LTBP-49247, we turned our attention to its potential safety profile. Previous studies have indicated severe cardiac toxicities in mice, rats, and cynomolgus monkeys with an antibody that inhibits all three TGF-β GFs (*7*) or with pharmacological ALK5 inhibition (*8*). These studies have also indicated other potential issues associated with targeting this pathway, including bleeding and hyperplasia in other tissues, such as the bladder.

Downloaded from https://www.science.org at Dalian University of Technology on November 13, 2025

A 13-week non–GLP (good laboratory practice) toxicology and toxicokinetic study was conducted in mice to assess the potential toxicity characteristics of LTBP-49247 (data file S1). Male and female CD1 mice were administered LTBP-49247 three times weekly by intraperitoneal injection at doses of 0 (vehicle), 10, 30, or 100 mg/kg for 13 weeks. Toxicokinetic parameters were calculated after day 1, day 29, and day 85 of dosing (data file S2). Concentrations of LTBP-49247 increased after a single dose on day 1 and decreased over the initial week of the study, likely because of target-mediated drug disposition. The exposure of LTBP-49247 increased after multiple doses, as assessed by comparing the accumulation ratio of the maximum exposure (C_{max}) and the area under the curve or $AUC_{(0–7)}$. At all doses tested, the C_{max} showed greater accumulation at day 85 compared with day 29 and day 1 quantities. The $AUC_{(0–7)}$ was only assessed after the first and last doses

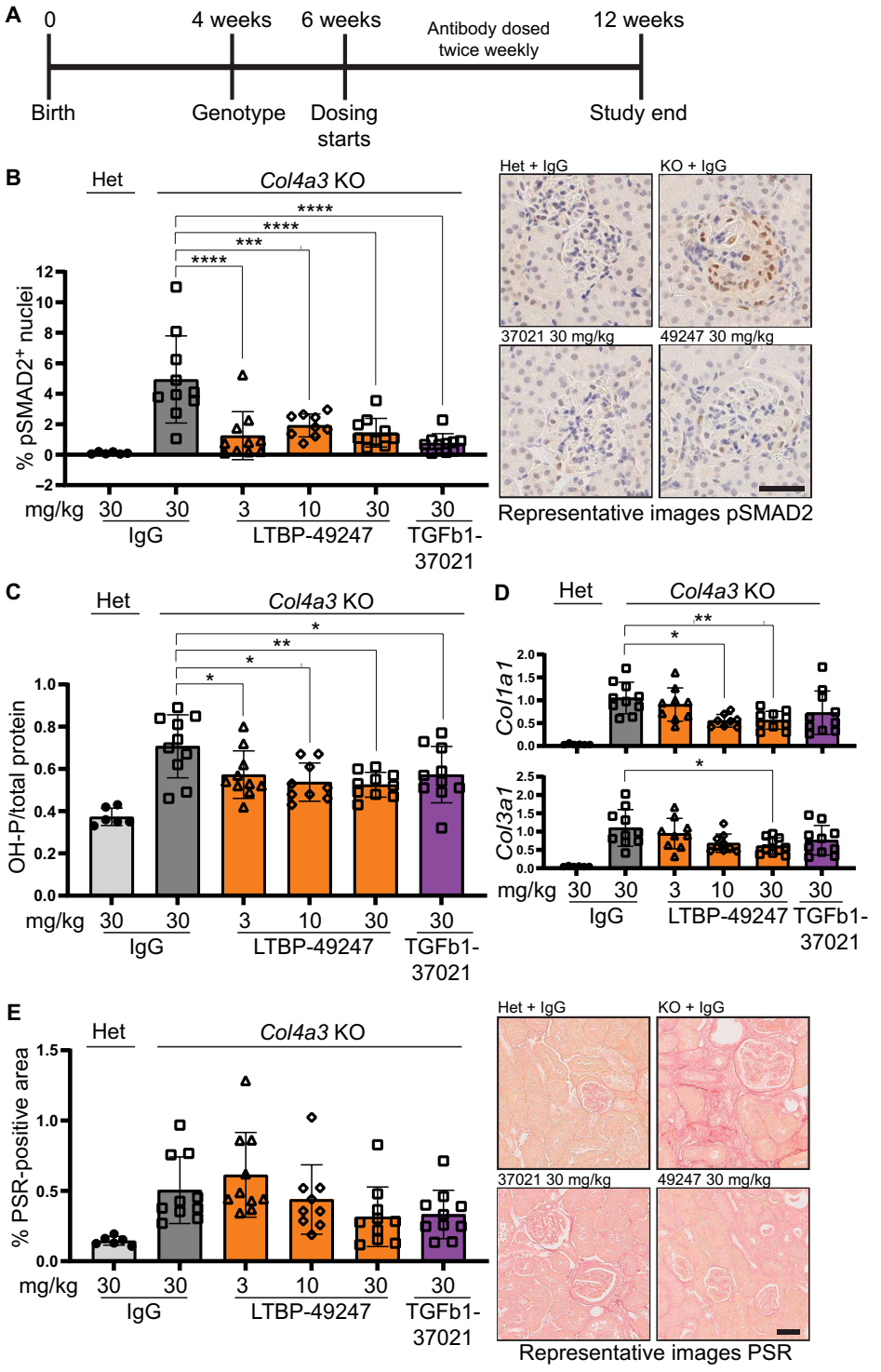

Fig. 5. LTBP-49247 suppresses fibrosis in a mouse model of Alport syndrome. (**A**) Experimental design for the kidney fibrosis study using the *Col4a3 KO* (*Col4a3*$^{-/-}$) mouse model of Alport syndrome. Col4a3$^{+/-}$ (Het) mice were used as a control comparator. Dosing with LTBP-49247, TGFb1-37021, or IgG (control) was initiated at 6 weeks of age and performed twice weekly until study termination at 12 weeks. (**B**) The graph shows the percentage of pSMAD2^{+} nuclei in kidneys as determined by quantitative immunohistochemistry at study termination. Representative group mean images show pSMAD2 in IgG control in both Het and *Col4a3 KO* mice, as well as the high-dose groups for both LTBP-49247–and TGFb1-37021–treated mice. Scale bar, 50 μm. (**C**) Percent hydroxyproline (OH-P) in kidneys normalized to total protein at study termination, as determined by biochemical methods. (**D**) Quantification of *Col1a1* and *Col3a1* expression in kidneys by quantitative polymerase chain reaction. (**E**) The graph shows the percent PSR^{+} area as determined quantitatively at study termination. Representative group mean images show PSR staining in IgG controls, high-dose LTBP-49247, and high-dose TGFb1-37021. Scale bar, 50 μm. For (B) to (E), statistical analysis was performed as follows: first, a robust regression and outlier removal (ROUT) test ($Q = 1\%$) was used to identify and remove outliers [two in (B), one in (C), zero in (D), and one in (E)], followed by a one-way ANOVA with comparison to IgG control–treated COL4A3 KO animals. Het controls animals were not compared in statistical analysis. *$P \leq 0.05$; **$P \leq 0.01$; ***$P \leq 0.001$; ****$P \leq 0.0001$. $n = 6$ Het control mice and $n = 10$ mice for each Col4a3 KO group. This study is representative of two independent studies with similar results.

Downloaded from https://www.science.org at Dalian University of Technology on November 13, 2025

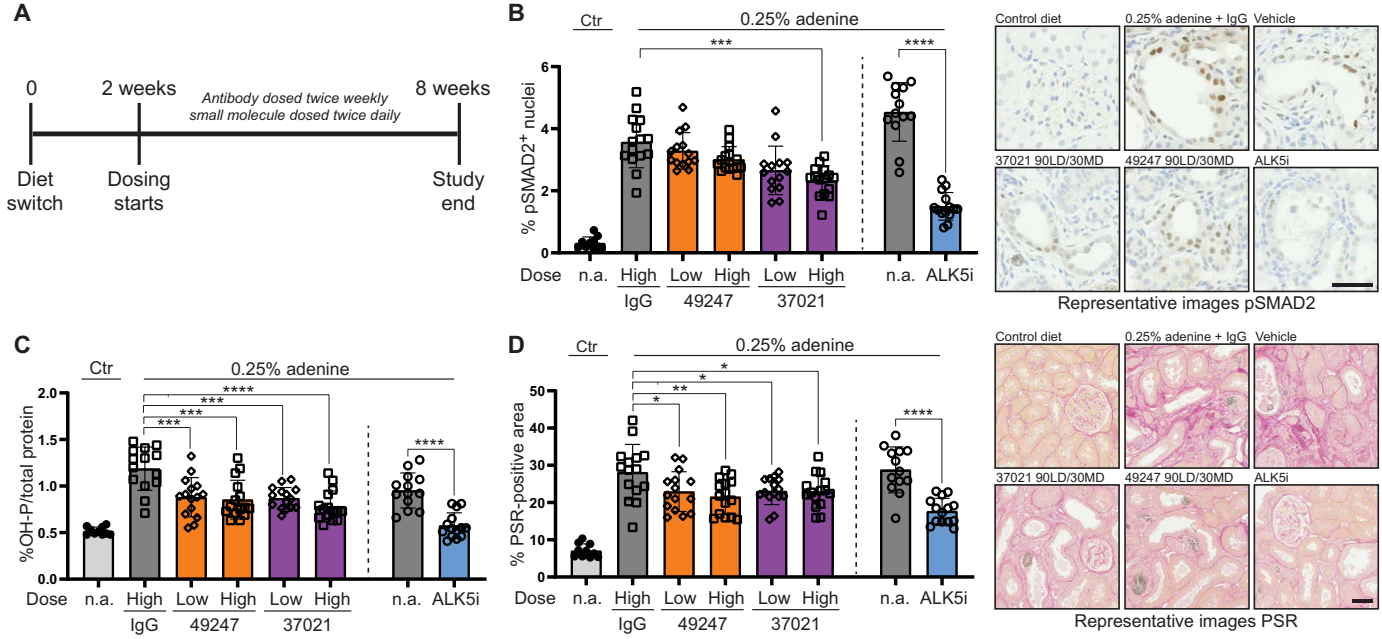

Fig. 6. LTBP-49247 is antifibrotic in a rat model of chronic kidney disease. (**A**) Experimental design of the rat model of adenine-induced kidney disease. After 2 weeks on a 0.25% adenine diet to induce tubular injury in the kidney, dosing with antibodies occurred twice weekly by intraperitoneal delivery or twice daily orally for vehicle and the small-molecule ALK5 inhibitor (ALK5i). For antibody treatments, an initial loading dose of 90 mg/kg (for doses of 30 mg/kg) and 30 mg/kg (for doses of 10 mg/kg) was used to maintain consistent antibody concentration in serum. The two dose schemes are indicated as "high" and "low" below the *x* axes of the graphs in (B) to (D). The study was terminated and the kidneys harvested at 8 weeks. (**B**) Graph shows the percent of pSMAD2$^+$ nuclei as determined by quantitative immunohistochemistry at study termination. Images show representative group mean images for animals on a control diet and adenine-fed animals treated with IgG, high-dose LTBP-49247, high-dose TGFb1-37021, vehicle, or ALK5i. Scale bar, 50 μm. (**C**) Percent hydroxyproline (OH-P) normalized to total protein at study termination, as determined by biochemical methods. (**D**) The graph shows percent PSR$^+$ area as determined quantitatively at study termination. Representative group mean images show PSR staining in animals on control diet and in adenine-fed animals treated with IgG, high-dose LTBP-49247, high-dose TGFb1-37021, vehicle, or ALK5i. n.a., no test article. Scale bar, 50 μm. For (B) to (D), statistical analysis was performed as follows: First, a ROUT test ($Q = 1\%$) was used to identify and remove outliers [two in (B), zero in (C), and one in (D)], followed by a one-way ANOVA with comparison to IgG control–treated 0.25% adenine-fed animals for the antibody groups. A Student's *t* test comparing vehicle and ALK5i-treated groups was used to analyze these groups separately because the route of administration and drug modality were different from the antibody groups. *$P \leq 0.05$; **$P \leq 0.01$; ***$P \leq 0.001$; ****$P \leq 0.0001$. $n = 10$ rats in the control diet group and $n = 15$ rats for each of the 0.25% adenine diet groups. This study is representative of two independent studies with similar results.

but showed consistent accumulation of LTBP-49247 at each dose. The overall magnitude of accumulation was less than dose proportional. The serum concentrations of LTBP-49247 achieved were well above the concentrations necessary for target engagement and antifibrotic effect in Alport and rat adenine fibrosis models. In addition, these concentrations are comparable to those seen in the previous study in which severe toxicities were observed with a pan–TGF-β inhibitor (*7*).

There were no test article–related effects on mortality, detailed clinical observations, body weight, food consumption, ophthalmoscopic examinations, hematology, coagulation, urinalysis, organ weights, or macroscopic examinations. Minor clinical chemistry effects were observed in males and females at 100 mg/kg per dose three times per week (i.e., 300 mg/kg per week), including mild increases in mean globulin concentration (up to 1.25×) and decreases in albumin/globulin ratio (as low as 0.79×). The globulin increases were considered likely because of administration of a high dose of immunoglobulin and an inflammatory response to microscopic peritoneal inflammation. Test article–related microscopic findings were limited to an increased incidence and/or severity of minimal to marked mixed cell inflammation in the Harderian gland in females at ≥30 mg/kg per dose and in males at 100 mg/kg per dose. Harderian gland inflammation is often associated with minimal degeneration or necrosis, and a male with marked mixed cell inflammation had more pronounced (moderate) degeneration or necrosis with loss of glandular tissue. Moderate or marked mixed cell inflammation in the Harderian gland is considered adverse to mice; however, humans do not have a Harderian gland, and these findings are not considered clinically relevant. Overall, these findings indicate that LTBP-49247 demonstrates none of the cardiac or noncardiac toxicities traditionally associated with TGF-β pathway inhibitors.

DISCUSSION

TGF-β is a central driver of fibrotic disease progression, but inhibition of the TGF-β pathway has historically resulted in toxicities that have proven severe and dose limiting (*7*, *8*). We previously demonstrated that selective inhibition of the activation of TGF-β1, while sparing TGF-β2 and TGF-β3 signaling, is an effective strategy to overcome primary resistance to checkpoint blockade in preclinical oncology models (*15*), while avoiding the toxicities observed with less selective TGF-β inhibitors (*14*). We hypothesized that selectively targeting LTBP-presented TGF-β1 could avoid immune cell activation but retain the antifibrotic effect of a TGF-β inhibitor, thereby fine-tuning TGF-β1 inhibition for the treatment of fibrosis.

Downloaded from https://www.science.org at Dalian University of Technology on November 13, 2025

Our data presented here show that LTBP-49247, a monoclonal antibody that inhibits only a subset of TGF-β1, may offer a superior approach compared with other TGF-β pathway inhibitors for the treatment of fibrosis. LTBP-49247 bound to and inhibited the activation of LTBP-complexed TGF-β1 and did not bind to GARP- or LRRC33-complexed TGF-β1. LTBP-49247 did not bind to or inhibit TGF-β2 or TGF-β3 and showed none of the cardiac liabilities reported previously for broader pathway inhibition (*7*) nor inflammations of other tissues such as gingiva, tongue, and esophagus (*42*).

Some studies indicate a key role for TGF-β2 signaling in the progression of fibrosis, with conflicting results for TGF-β3 as being both a driver and suppressor of fibrosis in different contexts (*43*–*46*). Although additional inhibition of TGF-β2 and/or TGF-β3 could potentially increase antifibrotic efficacy, such an approach may be problematic because it could introduce safety liabilities that have been observed with less specific pathway inhibitors. The data presented here suggest that inhibiting TGF-β1 alone is sufficient to drive an antifibrotic effect in two models of renal fibrosis of different etiologies.

The degree to which the various presentation contexts of TGF-β1 govern the regulation of different biological processes remains incompletely understood. Preclinical data suggest that immune exclusion and/or immune suppression in oncology involves TGF-β1 originating from multiple sources, including T_{reg} and endothelial cells (*47*), ECM (*48*), and tumor-associated macrophages (*49*). In fibrosis, however, it has been postulated that the ECM is likely a critical source of TGF-β1 through presentation by LTBPs (*50*). Our results support this idea because the LTBP–TGF-β1–targeting antibody LTBP-49247 achieved a similar reduction in renal fibrosis compared to the context-independent TGF-β1–targeting antibody TGFb1-37021. Our data indicate that the fraction of TGF-β1 signaling originating from LTBP complexes is different across the two models of fibrosis examined. In the Alport model, $pSMAD2^+$ nuclei and fibrosis were reduced similarly by LTBP-49247 and TGFb1-37021, which suggests that LTBP–TGF-β1 is the primary source of TGF-β1 signaling in this model. Conversely, LTBP-49247 showed minimal suppression of pSMAD2 in the rat adenine model compared with TGFb1-37021 even though both antibodies demonstrated similar attenuation of fibrosis. In this model, LTBP-49247 is evidently targeting a minor fraction of the total TGF-β1 signaling, and yet it was sufficient to reduce fibrotic progression. The rat adenine model may have a higher amount of GARP–and/or LRRC33–TGF-β1 signaling, but inhibition of these TGF-β1 complexes did not result in further antifibrotic activity compared to inhibition of LTBP-complexed TGF-β1 alone.

The discovery and engineering of LTBP-49247 required the identification of an antibody with multiple key properties. The binding epitope must not be present on TGF-β2 or TGF-β3 latent complexes and must also be unavailable on GARP–and LRRC33–TGF-β1 complexes. Crucially, the antibody must potently inhibit the integrin-mediated activation of latent LTBP complexes of TGF-β1 and ideally also inhibit protease-mediated activation of these complexes. Numerous phage and yeast display campaigns, including more than a dozen panning rounds of affinity maturation using large latent complexes of TGF-β, were necessary to achieve these characteristics. The structural studies performed herein identify this epitope and provide a potential explanation for the selectivity to LTBP–TGF-β1 complexes achieved and demonstrated in our biochemical experiments.

First, these studies demonstrate the inhibitory mechanism and specificity of LTBP-49247 for TGF-β1 as opposed to TGF-β2 and TGF-β3. The LTBP-49247 Fab bound to the TGF-β1 LAP N-terminal α helix and GF finger. This bipartite binding interface speaks to the mechanism of inhibition of activation of TGF-β1 by LTBP-49247 because this interaction stabilizes the latent complex and prevents dissociation of the GF from the LAP either by integrins or proteases. The LTBP-49247 Fab interacts with residues from TGF-β1 that are unique to TGF-β1 compared with TGF-β2 and TGF-β3, which accounts for the specificity observed in binding experiments and cell-based activity assays.

Second, our structural studies suggest a mechanism for the selectivity for LTBP–TGF-β1 complexes. LTBP-49247 bound in a region of the TGF-β1 complex that is near the attachment site for the four known presenting molecules. The available GARP–TGF-β1 and LRRC33–TGF- β1 (*23*, *24*) complex structures suggest that there would be either steric clashes between these presenting molecules and LTBP-49247 bound to TGF-β1 or that the epitope residues adopt a conformation incompatible with LTBP-49247 binding when TGF-β1 is presented by GARP or LRRC33. GARP and LRRC33 are likely negative specificity filters that exclude the ability of LTBP-49247 to bind to TGF-β1. The only structural information regarding LTBP1 or LTBP3 we are aware of is a nuclear magnetic resonance structure of the TGF-β–presenting domain (TB3 domain) from LTBP1 in isolation (*22*), which does not inform about the structure of TGF-β1. LTBP proteins are strings of epidermal growth factor (EGF) and TGF-β binding (TB) domains arranged similar to beads on a string, whereas GARP and LRRC33 proteins are composed of multiple LRR motifs that pack together into a single horseshoe-shaped domain. On LTBPs, TGF-β1 is presented within the relatively small TB3 domain where the presenting cysteine residues are in close proximity (1- to 4-Å separation in PBD: 1KSQ). Conversely, TGF-β1 appears to form an extensive interface with GARP and LRRC33 because the TGF-β1 interface spans several LRR motifs to cysteine residues separated by 24.7 Å on GARP (PBD: 6GFF) and 26.5 Å on LRRC33 (PBD: 7Y1R) (*51*). This lesser or nonexistent interface on LTBP proteins likely enables a high degree of conformational flexibility between LTBP and TGF-β1. We hypothesize that this greater conformational flexibility is why LTBP-49247 can bind LTBP-presented TGF-β1 complexes, whereas LRRC33 and GARP exclude access to the epitope for LTBP-49247.

The studies described here focused on LTBP1 and LTBP3 as the most likely presentation molecules of TGF-β1 in the context of fibrosis. Of the four LTBP molecules, LTBP2 lacks the TB3 domain necessary for presentation of TGF-β (*52*) and can be excluded as a relevant presentation context for TGF-β1. By comparison, LTBP4 contains this domain, but the complex of LTBP4–TGF-β1 forms poorly in vitro (*53*), which makes use in biochemical experiments challenging. Nonetheless, the mechanism we propose for the binding of LTBP-49247 suggests that it may also inhibit complexes of LTBP4–TGF-β1, which could be relevant in future studies or in different biological contexts.

Currently available treatment options for fibrosis are of modest and/or inconsistent efficacy, although a newer, more-targeted set of molecules is currently in clinical development with some promising early results (*54*). Some of these, such as the integrin $\alpha_v\beta_1$ and/or integrin $\alpha_v\beta_6$ inhibitors, are designed to suppress the activation of a subset of TGF-β signaling in fibrotic tissue to avoid the safety liabilities described above (*55*, *56*, *57*). Although these approaches are intriguing, we suggest that our approach may represent an even more selective suppression of TGF-β signaling because $\alpha_v\beta_6$ integrin has been shown to activate both TGF-β2 and TGF-β3 in some contexts (*58*, *59*) and has demonstrated safety issues both preclinically and clinically (*60*, *61*). In addition, our strategy also inhibits protease-mediated activation of TGF-β1, which is

Downloaded from https://www.science.org at Dalian University of Technology on November 13, 2025

likely unaffected by integrin-targeted strategies. In summary, specifically targeting LTBP–TGF-β1 demonstrates both an antifibrotic effect and favorable safety profile, suggesting that this may be an attractive approach for chronic administration as a treatment for organ fibrosis.

MATERIALS AND METHODS

Recombinant protein expression and purification

Recombinant proteins were expressed in Expi293F cells (Thermo Fisher Scientific) transiently transfected with pTT5 plasmids (National Research Council Canada) containing the DNA of interest. TGF-β LLCs were generated by cotransfecting Expi293F cells with a plasmid encoding proTGF-β1, proTGF-β2, or proTGF-β3 and a plasmid encoding an LLC-forming presenting molecule. LTBP fragments that contain the TGF-β–binding TB3 domain and flanking EGF-like domains were used to improve yields and protein quality over full-length LTBPs (Glu^{873} to Ile^{1507} for human LTBP1 and Asp^{866} to Glu^{1039} for human LTBP3). The LTBP fragments had a C-terminal His-tag to facilitate purification. Stable Expi293F cell lines were made that expressed C-terminally His-tagged GARP or LRRC33 ectodomains. These stable cells were transiently transfected with a plasmid encoding proTGF-β1 to generate GARP or LRRC33 LLCs with latent TGF-β1. The TGF-β SLCs were expressed with an N-terminal His-tag and the LLC-forming cysteine mutated to serine (C4S in TGF-β1) (*62*). Transfectants were cultured in Expi293 Expression medium (Thermo Fisher Scientific) for 5 days before the conditioned supernatant was collected. Recombinant proteins were purified by Ni^{2+} affinity chromatography, followed by size exclusion chromatography (SEC). Protein quality and formation of disulfide linked complexes were confirmed by SDS-PAGE and analytical SEC. Antibodies, including LTBP-49247 and TGFb1-37021, were expressed by cotransfection of Expi293F cells with pTT5 plasmids encoding heavy and light chains of interest. Human IgG4 (hIgG4), mouse IgG1 (mIgG1), and rat IgG1 (rIgG1) antibodies were purified by protein A capture, followed by SEC. High-salt and pH conditions (3 M NaCl at pH 8.6) were used to facilitate rIgG1 binding to protein A. The active TGF-β GFs were purchased from R&D Systems. The sequence of 1D11 was found in US Patent 10766955, and protein was produced internally or purchased from BioXCell (#BE0057). The antibody STX-100 was produced using the sequence available in the Global Substance Registration System, entry JD43Y6YF3N.

LLCs of TGF-β1 were biotinylated before performing SPR and MSD-SET experiments using either EZ-link sulfo–NHS (*N*-hydroxysulfosuccinimide)–biotin (Thermo Fisher Scientific) or the lighting link type B biotinylation kit (Novus Biologicals, 371-0010). The degree of labeling was determined using the QuantTag Biotin Quantitation Kit (Vector Laboratories).

Biolayer interferometry experiments (octet)

LTBP-49247 binding to various forms of TGF-β was measured by biolayer interferometry on a FortéBio Octet Red384 using polystyrene 96-well black half-area plates (Greiner Bio-One). Binding of LTBP-49247 hIgG4 to human proTGF-β1 C4S and human mature GFs TGF-β1, TGF-β2, and TGF-β3 was tested using amine reactive tips (AR2G, Sartorius). Amine reactive tips were preincubated in Milli-Q water before the initiation of an experiment for at least 10 min. In the first step of the experiment, tips are placed into water for 1 min, followed by an incubation with freshly prepared activation solution {18 parts of water, 1 part of 400 mM EDC [1-ethyl-3-(3-dimethylaminopropyl)carbodiimide], and 1 part of 200 mM sulfo-NHS} for 5 min, followed by the loading of TGF-β antigens, which was performed at 10 μg/ml in sodium acetate buffer (pH 5) for 3 min. Tips were then quenched with ethanolamine (pH 8.5) for 15 min, followed by a 20-min blocking step in 1× enhanced kinetics buffer (1× EKB) [Sartorius 1× kinetics buffer with the addition of 2% bovine serum albumin (BSA), 0.5 M NaCl, and 0.09% Tween 20). Last, binding of LTBP-49247 hIgG4 at 10 μg/ml (67 nM) in 1× EKB was tested with a 10-min association and a 10-min dissociation time. The EDC, NHS, sodium acetate buffer, and ethanolamine are part of the amine reactive reagents kit (Sartorius).

To test LTBP-49247 binding to human LTBP1–proTGF-β1, LTBP1–proTGF-β2, and LTBP1–proTGF-β3, anti-human Fc capture tips (AHC, Sartorius) were used. Tips were allowed to equilibrate in 1× EKB for at least 10 min before the start of the experiment, and EKB was used for all steps and dilutions in the experiment. Upon initiation of the experiment, a baseline of 2 min was performed in 1× EKB. Then, LTBP-49247 hIgG4 was immobilized to AHC biosensors for 300 s. A concentration of 0.5 μg/ml was used for this step. A second 2-min baseline step was performed, followed by association of the test antigens (LTBP1 alone or in complex with TGF-β1, TGF-β2, or TGF-β3) at 10 μg/ml that was then performed for 300 s, followed by a 1200-s dissociation in 1× EKB. The orbital speed was 1000 rpm for all steps of the experiment.

SPR experiments (Biacore)

The Biacore 8000 SPR system was used to evaluate the binding affinity of the Fab of LTBP-49247 and TGFb1-37021 to all known human complexes of TGF-β1 (LTBP1, LTBP3, GARP, LRRC33, and the SLC). Biotin CAPture kit and sensor chips (Cytiva) were used in these experiments. A filtered buffer consisting of 10 mM Hepes, 150 mM sodium chloride, 3 mM EDTA, and 0.05% polysorbate 20 (HBS-EP) (Cytiva) was used as the running buffer.

First, three startup cycles were performed. For each startup cycle, biotin CAPture reagent was loaded with a contact time of 300 s at a flow rate of 2 μl/min, and then 10 nM biotinylated LLC was loaded for 180 s at a flow rate of 10 μl/min. Running buffer was flowed over the sensor chip as a mock analyte binding step with a flow rate of 30 μl/min, a contact time of 120 s, and a dissociation time of 60 s. Regeneration solution was then injected with a flow rate of 10 μl/min and a contact time of 120 s. Last, a standard wash step was performed with buffer. This sequence was performed a total of three times as described above, and then the cycles to be used for analysis were performed. The cycles for analysis were identical to the startup cycles except that after loading of the biotinylated LLCs, running buffer containing LTBP-49247 or TGFb1-37021 human Fab, titrated to 10, 5, 2.5, 1.25, 0.625, and 0 nM concentrations, was flowed over the sensor chip. The dissociation time was also 300 or 900 s for the analysis cycles as opposed to 60 s for this step in the startup cycles.

Analysis was performed using the Biacore Insight Evaluation software using the predefined method "multicycle kinetics using capture." The R_{max} for LTBP-49247 for each interaction was set to be equal to the R_{max} of TGFb1-37021 binding to that antigen.

MSD-SET experiments

The MSD-SET experiment was performed by mixing increasing concentrations of LTBP-49247 with a set concentration (25 nM) of biotinylated human, mouse, rat, and cynomolgus monkey LLCs of

Downloaded from https://www.science.org at Dalian University of Technology on November 13, 2025

TGF-β1 for 20 to 24 hours at room temperature. To measure the amount of free antigen remaining in the equilibrium solution, MSD standard plates (MSD) were coated with a 20 nM solution of LTBP-49247 in phosphate-buffered saline (PBS) for 30 min at room temperature or overnight at 4°C. The antibody-coated plates were then blocked with blocking buffer A (MSD) for 30 min at room temperature and washed with wash buffer (PBS, 0.1% BSA, and 0.05% Tween 20) before adding the equilibrated LTBP-49247–antigen complexes to the plate for exactly 2.5 min. The plate was washed again with wash buffer before adding SULFO-TAG-labeled streptavidin secondary reagent (250 ng/ml; MSD) in PBS with 0.1% BSA. After washing with wash buffer, plates were read in MSD read buffer (MSD) using the MESO QuickPlex SQ 120 (MSD). The binding data were processed by nonlinear curve fitting in Prism 7 software (GraphPad) to calculate equilibrium binding K_D values.

T_{reg} binding assay

Buffy coats (Research Blood Components) were obtained according to the American Association of Blood Banks guidelines for drawing donors with an institutional review board (IRB)–approved informed written consent form for each donor. $CD4^+$ T cells were magnetically separated (STEMCELL Technologies) from freshly collected human peripheral blood mononuclear cells, and then T_{reg} cells were sorted on the basis of $CD25^{hi}$ staining (clone BC96, Thermo Fisher Scientific, catalog no. 17-0259-42; RRID AB_1659682) and $CD127^{lo}$ staining (clone HIL-7R-M21, BD Biosciences, catalog no. 557938; RRID AB_2296056) using a Bio-Rad S3E cell sorter. T_{reg} cells were stimulated for 4 days with plate-bound anti-CD3 clone OKT3 (10 μg/ml for plate coating; BioLegend, catalog no. 317301; RRID AB_571926) and soluble anti-CD28 clone 28.2 (10 μg/ml; BioLegend, catalog no. 302901; RRID AB_314303) in TexMacs medium (Miltenyi) with human interleukin-2 (100 ng/ml; Peprotech, catalog no. 200-02).

Separate staining tests were then run with 30 μg/ml of each antibody: HuNeg negative control, TGFb1-37021, LTBP-49247, and MHGARP8. Samples were run on an Attune NxT (Thermo Fisher Scientific) flow cytometer and analyzed by FlowJo (BD Biosciences). These antibodies were labeled with Alexa Fluor 488 NHS Ester (Thermo Fisher Scientific) according to the manufacturer's recommended protocol to enable their use in this study.

Integrin- and kallikrein-mediated TGF-β activation assays

To measure the inhibition of LTBP-presented TGF-β activated by integrin $\alpha_v\beta_8$, we used LN229 cells [American Type Culture Collection (ATCC), catalog no. CRL-2611] as previously described (*15*). To measure the inhibition of LTBP-presented TGF-β activated by integrin $\alpha_v\beta_6$, we used SW480 cells (ATCC, catalog no. CCL-228) stably expressing the integrin subunit β_6 (the α_v subunit is highly and ubiquitously expressed). These cells are referred to in the manuscript as SW480/b6 and were selected by Gly^{418} treatment and single-cell subcloning after transfection with a pcDNA3.1/neo plasmid containing the reading frame of integrin β_6. Both LN229 and SW480/b6 assays use the same protocol for measuring activity, differing only in the initial plating concentration of the cells. Briefly, 2 days before the assay, 12,500 LN229 or 15,000 SW480/b6 cells per well were plated into white-walled 96-well tissue culture–treated assay plates. Cells were transfected the next day with plasmids encoding proTGF-β1 (or proTGF-β2 or proTGF-β3 for the control experiment in fig. S3) using Lipofectamine 3000. Twenty-four hours later, the antibodies indicated were serially diluted and added to the transfected LN229 cells together with CAGA12 cells (derived from MvLu1 cells from ATCC, catalog no. CCL-64; stably transfected with a TGF-β promoter–based luciferase reporter cassette; and maintained with puromycin selection) at 15,000 cells per well suspended in Dulbecco's modified Eagle's medium (DMEM) + 0.1% BSA. Sixteen to 20 hours after setting up this coculture, the assay was developed for 2 min using BrightGlo reagent, and luminescence was detected on a PerkinElmer Envision plate reader. The data are normalized to luciferase activity in presence of antibody vehicle equal to 1.00. Dose-response curves were fit to a nonlinear three-parameter log inhibitor versus response model using GraphPad Prism.

To test the inhibition of proteolytic TGF-β1 activation, CAGA12 reporter cells were seeded into white-walled 96-well tissue culture–treated assay plates (12,500 cells per well). Twenty-four hours later, cells were washed with assay medium (DMEM + 0.1% BSA). Mixtures of the TGF-β1 SLC (130.7 ng/μl) with various antibodies (isotype control, 1D11, TGFb1-37021, and LTBP-49247, all at 3268.0 ng/μl) were incubated for 1 hour at room temperature in volumes of 45.9 μl. After incubation, 2 μl of kallikrein (0.15 mg/ml; EMD Millipore) or 2 μl PBS (for kallikrein control) was added to the SLC/antibody mixtures and incubated 2 hours at 37°C. From the SLC/antibody/kallikrein mixtures, 19.8 μl was diluted to 1 ml in assay medium, so the final concentration of the SLC was 2.5 ng/μl, and 50 μl of this dilution was added to the 50 μl of assay medium already present on the CAGA12 cells. The assay mixture was incubated with CAGA12 cells for ~18 hours, after which TGF-β1 activation was read out by bioluminescence on a PerkinElmer Envision and relative luminescence units were then plotted in GraphPad Prism. In parallel, 27 μl of the SLC/antibody/kallikrein mixtures was mixed with 9 μl of 4× SDS-PAGE sample buffer (Bio-Rad) and heated for 5 min. Two identical SDS-PAGE gels were run (with 500 ng of the SLC per lane); one gel was stained with Sypro Ruby (Invitrogen) according to the manufacturer's instructions, and the second gel was transferred to polyvinylidene difluoride (PVDF) membrane with a Bio-Rad Trans Blot Turbo according to the manufacturer's instructions. The PVDF membrane was blocked with 5% blocking reagent (Bio-Rad) dissolved in tris-buffered saline + 0.05% Tween (TBST; Boston BioProducts) for 1 hour at room temperature. The membrane was probed with anti-LAP plasma kallikrein degradation fragment L59 monoclonal antibodies, clone 6D6 (Cosmo Bio) (*63*) diluted to 50 ng/ml in 1% blocking reagent in TBST overnight at 4°C. The membrane was washed three times for 5 min in TBST. The membrane was probed with goat anti-mouse horseradish peroxidase (HRP)–conjugated secondary antibody (R&D Systems) diluted 1:10,000 in 1% blocking reagent in TBST. The membrane was washed three times for 5 min, then incubated with enhanced chemiluminescence reagent (Bio-Rad) according to the manufacturer's instructions, and imaged.

Crystallography protein expression and sample preparation

The human TGF-β1 gene was cloned into the Eco RI and Not I restriction sites of the pTT5 plasmid; however, the native secretion signal sequence was replaced with that from the Igκ chain (MDMRVPAQLLGLLLLWFSGVLG). In addition, Cys^{33} (UniProt numbering; or Cys^4 in mature protein) was mutated to serine to prevent complex formation with presenting molecules, and Arg^{278} (UniProt numbering; or Arg^{249} in mature protein) was mutated to alanine to disrupt the furin protease cleavage site and prevent cleavage between the LAP and the mature GF (*18*). This protein is referred to as TGF-β1 C4S, furin

Downloaded from https://www.science.org at Dalian University of Technology on November 13, 2025

mutant and remains an "obligate" latent complex because the GF cannot dissociate from the LAP.

The LTBP-49247 hIgG1 Fab was cloned by inserting DNA encoding the mIg heavy-chain V region 102 signal peptide (MGWSCIILFLVATATGAHS), followed by the 49247 VH domain, the hIgG1 CH1 domain, and a six-histidine affinity tag into the Eco RI and Bam HI restriction sites of pTT5. The LTBP-49247 lambda light chain was cloned by inserting DNA encoding the mIgG heavy chain V region 102 signal peptide, followed by the 49247 VL domain and the human lambda CL domain into the Eco RI and Bam HI restriction sites of pTT5.

The TGF-β1 C4S, furin mutant was coexpressed with the LTBP-49247 Fab in in 12 liters of Expi293 GnTI$^-$ cells (Thermo Fisher Scientific) in Dynamis expression medium (Thermo Fisher Scientific) with a 1:1:1 ratio of TGF-β1:heavy-chain:light-chain DNA. Expi293 GnTI$^-$ cells were seeded at 0.6×10^6 cells/ml. Two days later, when the cell density was 2.5×10^6 to 2.6×10^6 cells/ml (98% live), transfection was performed by adding 1 mg of total DNA per liter of cells (equal amounts of pTT5–TGF-β1 C4S, furin mutant, pTT5-49247 Fab heavy chain, and pTT5-49247 light chain) to Dynamis medium. Separately, polyethyleneimine (PEI; 2.88 mg/ml) "max" (0.22-μm filtered; Polysciences, #24765) was mixed with 100 ml of Dynamis medium per liter of cells. Both DNA and PEI dilutions were incubated 5 min at room temperature. The PEI solution was transferred to DNA solution and incubated for 5 min at room temperature. The DNA:PEI mixture was added to the cells, and cells were returned to 37°C incubator with shaking. Twenty-four hours after transfection, cells were fed with 25 ml of 20% (w/v) of Tryptone N1 and 40% (w/v) of glucose (dissolved in Dynamis medium and 0.22-μm filtered) per liter of cells. Four days after feeding, conditioned medium was harvested by centrifuging cells for 20 min at 6900*g* at 4°C and filtering the supernatant with a 0.22-μm filter and stored with 0.025% sodium azide at 4°C until purification.

The conditioned medium was adjusted to 50 mM tris-HCl and 0.5 M NaCl with the addition of 1 M tris (pH 8.0) and 5 M NaCl. The pH was adjusted to pH 8.0 with NaOH and filtered. The TGF-β1:LTBP-49247 Fab complex was affinity captured by immobilized metal affinity chromatography (IMAC) by batch binding with Ni–nitrilotriacetic acid (NTA) resin (QIAGEN) as follows. To the adjusted conditioned medium, nickel sulfate was added to 0.5 mM, from a 0.1 M stock, and a 50% slurry of Ni-NTA beads, equilibrated with 20 mM phosphate and 0.5 M NaCl (pH 8.0), was added (5 ml of Ni-NTA slurry per liter of conditioned medium) and mixed overnight at 4°C. The beads were collected with gravity filtration to a column and washed with 20 mM phosphate and 0.5 M NaCl (pH 8.0). Protein was eluted in 20 mM phosphate, 0.5 M NaCl, and 0.5 M imidazole (pH 7.8). The Ni-NTA elution fractions were pooled and further purified on Superdex 200 26/600 SEC, with 20 mM Hepes and 150 mM NaCl (pH 7.5) (HBS, pH 7.5) mobile phase to separate the TGF-β1/Fab complex from free Fab. The complex was concentrated to 10 mg/ml, aliquoted in 50 to 100 μl of aliquots, flash-frozen in liquid nitrogen, and stored at −80°C for later use. This batch was used for initial crystallization screens and refinement of initial hits.

In a subsequent complex purification, 12 liters of conditioned medium containing the TGF-β1 C4S, furin mutant alone [generated from expression in Expi293 GnTI$^-$ cells as described above (1 mg of pTT5–TGF-β1 C4S DNA per liter of cells)] was mixed with 6 liters of conditioned medium containing the 49247 Fab [generated from expression in Expi293 cells as described above (1 mg of total DNA per liter of cells, with 1:1 ratio of heavy chain to light chain)]. The complex from this mixed conditioned medium was purified the same way as the TGF-β1 C4S, furin mutant coexpressed with the LTBP-49247 Fab described above. This batch was used for the further crystallization refinement and was the source material in the crystal for the structure dataset.

Crystallography

The TGF-β1 C4S, furin mutant/49247 Fab complex (10 mg/ml) was mixed with papain (1 mg/ml) at a ratio of 10:1 (v/v) and incubated on ice for 2 hours. Initial crystal hits were obtained in 15% polyethylene glycol (PEG) 3350 and 11% tacsimate (pH 4.0) in sitting drop vapor diffusion experiments set by mixing 100 nl of protein with 100 nl of well solution. This condition was screened with various additives (Hampton Research), and crystals grown in 15% PEG 3350, 12% tacsimate (pH 4.0), and 10 mM $MgCl_2$ gave the best diffraction. The crystals were cryoprotected with 15% PEG 3350, 12% tacsimate (pH 4.0), and 10% glycerol before flash-freezing in liquid nitrogen.

X-ray diffraction data collection and structure determination

Crystals were diffracted at the Advanced Photon Source 23ID-D beamline. Data were processed with x-ray detector software (XDS) (*64*). A molecular replacement solution for the complex was solved with a TGF-β1 homodimer (5FFO) and two Fabs (7JVC) using Phaser 2.8.3 software (*65*). The model was improved with successive rounds of manual building and refinement with Coot 0.9.6 (*66*) and Refmac 5.8 (*67*). The relevant crystallographic statistics are present in table S1.

H/DX sample preparation

To isolate the preformed complex of human LTBP1–TGF-β1/49247 Fab complex, a 1:2 molar ratio of human LTBP1–TGF-β1:49247 Fab was incubated for 1 hour at room temperature. The protein complex was then injected onto a Superdex 200 Increase 10/300 GL column using 20 mM Hepes and 150 mM NaCl (pH 7.5) as the mobile phase. The peak fraction containing the human LTBP1–proTGF-β1/LTBP-49247 Fab was pooled, concentrated, filtered, and subjected to H/DX-MS.

H/DX reaction

H/DX experiments were performed using a preformed complex of human LTBP1–TGF-β1/49247 Fab (15-μM) in sample buffer [20 mM Hepes and 150 mM NaCl (pH 7.5)]. A 15 μM human LTBP1–TGF-β1 only was also prepared for the unbound antigen control. The protein samples were incubated at room temperature for 1 hour and then introduced into the nanoACQUITY system (*68*) equipped with H/DX technology for ultraperformance liquid chromatography (UPLC) separation (Waters Corp., Milford, MA), which performed all subsequent manipulations for the H/DX. H/DX was initiated by dilution of each sample 15-fold with H/DX buffer [20 mM Hepes and 150 mM NaCl (pH 7.5)], and the mixture was incubated at predetermined H/DX time points (0.17, 1, 10, 60, and 120 min) at 25°C. At the indicated H/DX time point, an aliquot from the exchange reaction was removed, and deuterium labeling was quenched by adding equal volume of quench buffer [100 mM phosphate, 4 M guanidine-HCl, and 0.5 M tris(2-carboxyethyl) phosphine (TCEP) (pH 2.5)] at 3°C. For the nondeuterated samples, the same procedure was performed in H_2O buffers. Quenched samples were introduced into a 5-μm ethylene bridged hybrid (BEH) 2.1-mm by 30-mm Enzymate-immobilized pepsin column (Waters Corp., Milford, MA) at 100 μl/min in 0.1% formic acid at 10°C and

Downloaded from https://www.science.org at Dalian University of Technology on November 13, 2025

then incubated for 4.5 min to allow on-column digestion. Peptide fragments were collected at 0°C on a C18 VanGuard trap column (1.7 μm by 30 mm) (Waters Corp., Milford, MA) for desalting with 0.1% formic acid in H_2O and were then separated using a 1.8-μm high strength silica (HSS) T3 C18 2.1-mm by 30-mm nanoACQUITY UPLC column (Waters Corp., Milford, MA) for a 10-min gradient from 0.1% formic acid to acetonitrile (7 min, 5 to 35%; 1 min, 35 to 85%; 2 min hold, 85% acetonitrile) at 40 μl/min at 0°C. Fragments were subsequently mass analyzed using Synapt G2Si ESI-Q-Tof mass spectrometer (Waters Corp., Milford, MA). In between sample injections, a wash step using pepsin wash buffer was performed to minimize peptide carryover.

Data processing for H/DX-MS

Accurate mass and collision-induced dissociation in data-independent acquisition mode (MSE) (*69*) and ProteinLynx Global Server (PLGS) 3.0 software (Waters Corp., Milford, MA) were used to determine the peptic peptides in the undeuterated protein samples analyzed on the same UPLC-ESI-QToF system used for H/DX-MS experiments. Peptic peptides generated from PLGS were imported into DynamX 3.0 (Waters Corp., Milford, MA) with peptide quality thresholds of an MS1 signal intensity of ≥1000 and a maximum mass error of 1 part per million. Automated results were manually inspected to ensure that the corresponding mass/charge ratio and isotopic distributions at various charge states were properly assigned to the appropriate peptic peptide. DynamX 3.0 was then used to generate the relative deuterium incorporation plot and H/DX heatmap for each peptic peptide. The relative deuterium incorporation of each peptide was determined by subtracting the weight averaged centroid mass of the isotopic distribution of undeuterated control sample from that of the weight-averaged centroid mass of the isotopic distribution of deuterium-labeled samples at each labeling time point. All comparisons were performed under identical experimental conditions, thus negating the need for back exchange correction in the determination of the deuterium incorporation. Therefore, the amount of H/DX is reported as relative (*70*). The fractional relative deuterium uptake was calculated by dividing the relative deuterium uptake of each peptic peptide by its theoretical maximum uptake. All H/DX-MS experiments were performed in duplicate, and a 98 = *n*% confidence limit for the uncertainty of the mean relative deuterium uptake of ±0.6 Da was calculated as described (*71*). Differences in deuterium uptake between two states that exceed 0.6 Da were considered significant.

Mouse model of Alport syndrome

Pharmacology studies using the mouse model of Alport syndrome were run at Hooke Laboratories in Lawrence, MA in compliance with Institutional Animal Care and Use Committee (IACUC) guidelines. For the representative studies presented in Fig. 5 and fig. S7, approval was granted under 2103PK-tolerance and 1703PK-tolerance, respectively. In these studies, male 129-Col4a3^{tm1dec}/J (originally from the Jackson Laboratory, strain #002908) heterozygotes were crossed with female Col4a3 C57BL/6 heterozygotes (derived from multiple rounds of backcrossing the 129-Col4a3^{tm1dec}/J with wild-type C57Bl/6 mice) to generate F1 homozygotes for dosing studies with the indicated antibodies. All genotyping was performed at 4 weeks of age, before initiation of any dosing regimens. For these studies, rolling enrollment of animals of both sexes was performed, with treatment groups balanced by sex and age. These F1 Col4a3 KOs live until 14 to 18 weeks of age before kidney failure and death. The timing of studies was therefore set up to achieve study termination before substantial mortality and loss of kidney integrity, which complicates analysis. For assessing target engagement by quantifying pSMAD2$^+$ nuclei in Alport model kidneys, F1 KO mice at 11 weeks of age were dosed intraperitoneally once with the indicated antibody test article before terminal blood draw and euthanasia with tissue collection 48 hours later. For multidose efficacy studies, KO mice at 6 weeks of age were dosed intraperitoneally twice weekly with the indicated antibody test articles for 6 weeks before terminal blood draw and euthanasia with tissue collection.

In the Alport studies, the antibodies were prepared on a mIgG1 backbone for the multidose study and on a hIgG4 backbone for the single-dose study. For the multidose studies, all antibodies were formulated in sterile 20 mM citrate and 150 mM NaCl (pH 5.5). In the single-dose study, isotype control and TGFb1-37021 were formulated in sterile PBS, whereas LTBP-49247 was formulated in 20 mM citrate and 150 mM NaCl (pH 5.5). In comparison with the PBS formulation used in rat adenine studies, citrate buffer does sometimes cause mild injection site irritation, but this was observed irrespective of test article (including IgG control) and was not considered to alter the results of the study. All antibodies were administered at 10 ml of dosing solution per kilogram of body weight.

To collect serum, blood was collected through the retro-orbital sinus into tubes containing a gel-clot activator. Kidney tissue collection procedures differed slightly between single and multidose studies. In the multidose study, the left kidneys were bisected coronally with one-half fixed in 10% neutral-buffered formalin for 24 hours before transferring to 70% ethanol for shipping. The other half of the left kidney, as well as both bisected halves of the right kidney, was immediately flash-frozen in liquid nitrogen before shipment to the final destination for analysis. For the single-dose study, the left kidney was flash-frozen whole in liquid nitrogen, whereas the right kidney was bisected with one-half flash-frozen in liquid nitrogen and the other half fixed in 10% neutral-buffered formalin for 24 hours before transferring to 70% ethanol for shipping.

Rat adenine model of kidney disease

The rat adenine model of chronic kidney disease was run at Inotiv-Westminster (formerly Plato BioPharma) in Westminster, CO in compliance with Inotiv-Westerminster's IACUC, which undergoes regular assessment of compliance. Male Spraque-Dawley rats were procured from Charles River Laboratories (stain code 001) and fed a control diet (Envigo/TD.170417) or a diet containing 0.25% adenine (Envigo/TD.180493) as indicated for the duration of the study. Briefly, the 0.25% adenine diet results in crystal deposits in the proximal tubules of the kidney, which impair kidney function and result in inflammation and fibrosis. For randomization of the treatment groups in the rat adenine studies, the following variables were used: day of dosing body weight, change in body weight from day of dosing compared with 2 weeks prior, blood urea nitrogen (BUN), and plasma creatinine.

Animals were dosed intraperitoneally with the indicated antibodies using the indicated dosing schemes (single dose or 2× weekly for 6 weeks, depending on the study) or with oral administration of the ALK5 inhibitor SB-525334 and vehicle control for this compound twice daily (morning and evening). For the single-dose studies, both TGFb1-37021 and LTBP-49247 were prepared on a hIgG4 backbone. For multidose studies, both TGFb1-37021 and LTBP-49247 were prepared on a rIgG1 backbone to reduce immunogenicity over the

Downloaded from https://www.science.org at Dalian University of Technology on November 13, 2025

course of the study. For these studies, antibodies were formulated in 20 mM tris and 150 mM NaCl (pH 8.0), and SB-525334 was formulated in aqueous 0.5% methylcellulose/0.5% Tween 80. For the multidose rat adenine study, a loading dose of 90 mg/kg was used for the dosing groups (30 mg/kg), and that of 30 mg/kg was used for the dosing groups (10 mg/kg) to maintain consistent concentration of the antibodies in serum throughout the study.

Serum collections were performed using conscious tail venous puncture and immediately flash-frozen in liquid nitrogen. Terminal tissue collections of the kidney were performed to accommodate both biochemical measurement of OH-P and histological examination of pSMAD2 and PSR. For biochemical analysis, the kidneys were immediately flash-frozen in liquid nitrogen and stored at −80 C until further analysis. For histological analysis, samples were immersed in 10% neutral-buffered formalin for 48 hours before transfer to 70% ethanol for shipment to the destination where analysis was performed.

Assays for concentrations of antibody in serum

A standard procedure was developed to detect the concentration of both LTBP-49247 and TGFb1-37021 in mouse and rat serum. The assay format used was a sandwich antigen capture enzyme-linked immunosorbent assay (ELISA) with a colorimetric readout. Briefly, a solution of streptavidin (2 μg/ml) in PBS was coated on a microtiter plate overnight. The following day, the plate was washed three times with a solution of 1× TBST and then blocked with BSA buffer, after which the biotinylated capture antigen complex, human LTBP1 at 0.5 μg/ml, was added to the plate. After wash, serum samples, standards, and quality controls [containing LTBP-49247 or TGFb1-37021 (hIgG4, rIgG1 or mIgG1)] were treated with acetic acid and then neutralized before being added to the plate. After a subsequent incubation, plate-bound antibody was detected by adding HRP-labeled goat anti-hIgG antibody at 1:10,000 in 1× TBST and detected with 3,3′, 5,5′-tetramethylbenzidine dihydrochloride (TMB) substrate. The plate was then read at 450 nm with a subtraction wavelength of 630 nm. The range of quantitation for this assay was 62.5 to 2000 ng/ml in neat serum (3.125 to 100 ng/ml in the assay plate well). The minimum required dilution for this assay was 1:20 (the assay is run in 5% serum).

RNA isolation and quantitative polymerase chain reaction

Total RNA was extracted from snap-frozen pulverized kidney tissue using TRIzol (Invitrogen, Carlsbad, CA), followed by RNeasy column (QIAGEN, Hilden, Germany) purification. The same method was used for analyzing gene expression from cell lines. Specific to characterization of gene expression in cell lines, THP-1 cells (ATCC, TIB-202) were used as a comparator for LN229 and SW480/b6 cells. cDNAs were synthesized with qScript cDNA Supermix synthesis kit (Quantabio, Beverly, MA) according to the manufacturer's instructions. Gene expression analysis was performed on duplicate samples with TaqMan (Applied Biosystems, Foster City, CA) technology using QuantStudio7 (Applied Biosystems) over 40 cycles. Expression data were normalized to glyceraldehyde-3-phosphate dehydrogenase mRNA expression, and $\Delta\Delta C_t$ method was used to calculate fold change. TaqMan sequences are available upon request.

Chromogenic pSMAD2 immunohistochemistry and PSR assay and analysis

pSMAD2 and PSR assays were run at Scholar Rock laboratories or at the laboratories at InVicro in Needham, MA. The protocol used in both laboratories was the same, with similar results for run controls across all studies.

Immunohistochemistry protocols were developed for chromogenic monoplex staining of kidney samples with pSMAD2 (Cell Signaling Technology, 3108S and 138D4). Staining was performed using a Leica Bond Rx staining system. Samples were collected and fixed in 10% neutral-buffered formalin for 24 hours at room temperature. Fixed samples were then stored in 70% ethanol until processed for paraffin infiltration and embedding. Paraffin-embedded samples were sectioned at 4 μm and mounted on slides for staining. pSMAD2 primary antibody was used at a final concentration of 0.044 μg/ml. Epitope retrieval was performed with a pH 9 (EDTA)–based solution and incubated at 100°C for 20 min. Slides were washed in a tris-based buffer, incubated with a peroxide blocking reagent, then washed three times in buffer, and incubated with a protein blocking reagent for 20 min before incubation with primary antibody for 60 min. Slides were again washed with buffer before incubation with a Leica HRP-polymer conjugate for 8 min. Slides were then washed twice more in buffer and once in deionized water before incubating with a Leica diaminobenzidine (*19*) chromogen for 10 min. Slides were then washed three times with deionized water and counterstained with hematoxylin for 5 min.

PSR staining protocol was adapted for automation using a commercial reagent system (Abcam, ab150681). Paraffin-embedded samples were sectioned at 4 μm and mounted on slides for PSR staining. Slides were baked at 60°C for 1 hour and deparaffinized through a series of xylenes and graded alcohols before rehydration in deionized water. Slides were then immersed in picrosirius red solution for 1 hour and filled by immediate rinsing in two changes of 0.5% acetic acid. Slides were then washed in 100% ethanol, followed by xylene before being coverslipped. Slide imaging was performed with a Zeiss Axio Scan.Z1 whole-slide scanning system, and spatial analysis was performed with Visiopharm custom-authored algorithms.

pSMAD2 image analysis used 8-bit thresholding of chromogen intensity within feature layers. 3,3'-Diaminobenzidine (DAB) staining for positive nuclei was separated from the hematoxylin-counterstained negative nuclei. Once these positive feature layers were established, cells were thresholded into light, medium, and strong positive signal bands to allow for fine-tuning of background elimination. Once these thresholds were established, all remaining positive channels were merged into a new mask representing the final array of object values. These object values retained information about their size, shape, and spatial coordinates within the overall image frame to quantify total cell positivity for pSMAD2 staining.

PSR image analysis thresholds were determined by average intensity values sampled from randomly distributed regions of fibrosis in control slides. Viable tissue area was broken down by pixel intensity and classified relative to previously determined thresholds for PSR positivity. Regions of glass, surrounded by tissue, with an area greater than 40 μm^2 were excluded from total tissue area calculations. Total positive pixel area was then divided by total tissue area to determine final PSR positivity.

PSR and pSMAD2 image analysis data were then transferred to GraphPad Prism, where the graphs for this manuscript were prepared. Statistical analysis described was performed in GraphPad Prism.

Fluorescent multiplexed pSMAD2/CD45/CD31 assay and analysis

Multiplex immunofluorescent assay protocol was developed at Scholar Rock for staining of the kidney samples with pSMAD2

Downloaded from https://www.science.org at Dalian University of Technology on November 13, 2025

clone E8F3R (Cell Signaling Technology, 18338), CD45 multiclone RM1007 (ab281586), and CD31clone 707 K3 (MA5-37858). Staining was performed using Leica Bond Rx staining system. Tissue preparation and sectioning were the same as described above for the chromogenic assay. Final concentrations of the antibodies were as follows: pSMAD2 (0.05 μg/ml), CD45 (0.0965 μg/ml), and CD31 (1.12 μg/ml). Epitope retrieval was performed with a pH 9 (EDTA) incubation at 100°C for 20 min. Slides were then washed in a tris-based buffer and then subjected to the following blocking/staining/washing/stripping sequence of steps repeated for each of the primary antibodies. First, slides were incubated with a protein blocking reagent for 30 min and then with the primary antibody for 60 min and, after that, washed with the buffer before incubation with ImmPRESS HRP goat anti-rabbit IgG polymer (Vector Laboratories) for 30 min. Slides were then washed in the buffer again, incubated for 10 min with an appropriate Opal reagent (tyramide conjugated fluorophore) (Akoya), and washed in the buffer again before being subjected to a stripping solution (citrate buffer, pH 6) at 95°C for 20 min. After the final buffer washes, the same sequence of steps was followed for the second antibody and then for the third. The order of primary antibodies in a staining sequence was first pSMAD2, second CD45, and third CD31. Opal 650 was assigned to pSMAD2, Opal 520 to CD45, and Opal 570 to CD31. At the end of the final sequence, slides were coverslipped using ProLong Gold mounting medium with 4′,6-diamidino-2-phenylindole. Slide imaging was performed with a Zeiss Axio Scan.Z1.

pSMAD2/CD45/CD31 image analysis was performed using the Phenoplex feature of Visiopharm software. After cell segmentation, thresholds were established for each fluorophore within built-in Phenoplex feature that allows us to visualize colocalization of markers (phenotypes) that can be quantitatively exported to GraphPad Prism for graphing and statistical analysis.

OH-P biochemical assay for fibrosis

Biochemical analysis of OH-P for both Alport and adenine studies was conducted at Inotiv-Westminster (formerly Plato BioPharma) in Westminster, CO. Cryogenically powdered renal tissue was subjected to biochemical analysis of OH-P as a surrogate marker of collagen. Tissue samples were weighed and lysed in deionized H_2O, and protein concentrations were determined by bicinchoninic acid (BCA) assay. Tissue lysates were hydrolyzed in 6 N of HCl and incubated at 110°C overnight. Hydrolysates were brought to room temperature and centrifuged at 16,100*g* for 5 min. A seven-point standard curve of OH-P was performed in duplicate for each assay. Hydrolysates and standards were added to separate wells of a 96-well plate and air-dried at room temperature until completely desiccated. Chloramine T solution was added to all wells and incubated at room temperature for 30 min with agitation. Ehrlich's reagent was then added to all wells, and the plate was sealed and incubated at 65°C for 40 min. The plate was brought to room temperature, and the absorbance was read at 560 nm using a Molecular Devices SpectraMax ABS Plus plate reader. Relative optical densities (ODs) were background-corrected against blank samples, and standard curves for the conversion of OD to concentration were generated using the four-parameter curve fitting method. Sample concentrations were determined using SoftMax Pro7.1 software (Molecular Devices) and corrected for dilutions as appropriate. Samples with OD values outside the linear range of the assay were repeated at an appropriate dilution. OH-P data were normalized to both tissue weight and total protein.

In vivo toxicology study in mice

For the toxicology and toxicokinetic study conducted in mice, LTBP-49247 hIgG4 was supplied at a concentration of 10 mg/ml and stored at −60° to −90°C. The vehicle was citrate-buffered saline [20 mM citrate and 150 mM NaCl (pH 5.5)] and stored at room temperature.

A non-GLP repeat dose toxicology and toxicokinetic study was performed in Crl:CD1 Institute for Cancer Research (ICR) mice (7 to 9.5 weeks old) at Charles River Laboratories Inc. This study was in compliance with all applicable sections of the Final Rules of the Animal Welfare Act regulations (Code of Federal Regulations, Title 9), the Public Health Service Policy on Humane Care and Use of Laboratory Animals from the Office of Laboratory Animal Welfare, and the Guide for the Care and Use of Laboratory Animals from the National Research Council. Male and female mice were group-housed (two or three per cage) for the duration of the study in solid bottom cages with nonaromatic bedding, an automatic watering valve, and a controlled environment (68° to 79°F, 30 to 70% relative humidity, and 12-hour light and dark cycles). Mice were offered standard rodent chow (Block Lab Diet) and tap water ad libitum. Mice were randomly assigned to treatment groups for all studies. The experimental design of the study is outlined in data file S2.

For safety evaluations, mortality and general cage side observations were performed twice daily (morning and afternoon). Postdose observations were performed once daily at 2 to 3 hours after dose to assess acute toxicity. Detailed clinical observations were performed weekly during the study and on the day of scheduled necropsy. Other observations performed included an assessment of body weight (weekly) and food consumption (weekly), ophthalmology (before scheduled necropsy), clinical pathology (hematology, serum chemistry, coagulation, and urinalysis), and anatomic pathology (gross and microscopic).

In vivo toxicokinetic study in mice

Serum samples were evaluated for LTBP-49247 with a sandwich antigen capture ELISA method with a colorimetric readout as described in the "In vivo toxicology study in mice" section above. The absorbance versus concentration relationship was regressed using a four-parameter logistic curve fitting, with a weighting factor of 1/Y2, and concentrations were calculated using GraphPad Prism or Watson LIMS (Thermo Fisher Scientific) data reduction software. The range of quantitation for this assay was 62.5 to 2000 ng/ml.

Toxicokinetic parameters were calculated in Phoenix WinNonLin 8.2.0.4383 from the concentration-time data using a noncompartmental analysis method. The C_{max} was calculated after the dose on days 1, 29, and 85. The $AUC_{(0–7)}$ was calculated over a week period after the doses on days 1 and 85.

Supplementary Materials

This PDF file includes:

Figs. S1 to S13
Tables S1 to S2

Other Supplementary Material for this manuscript includes the following:

Data files S1 and S2
MDAR Reproducibility Checklist

REFERENCES AND NOTES

1. X. Li, L. Zhu, B. Wang, M. Yuan, R. Zhu, Drugs and targets in fibrosis. *Front. Pharmacol.* **8**, 855 (2017).

Downloaded from https://www.science.org at Dalian University of Technology on November 13, 2025

2. S. L. Friedman, M. Pinzani, Hepatic fibrosis 2022: Unmet needs and a blueprint for the future. *Hepatology* **75**, 473–488 (2022).
3. X. M. Meng, D. J. Nikolic-Paterson, H. Y. Lan, TGF-β: The master regulator of fibrosis. *Nat. Rev. Nephrol.* **12**, 325–338 (2016).
4. E. H. Budi, J. R. Schaub, M. Decaris, S. Turner, R. Derynck, TGF-β as a driver of fibrosis: Physiological roles and therapeutic opportunities. *J. Pathol.* **254**, 358–373 (2021).
5. Y. Isaka, Targeting TGF-β signaling in kidney fibrosis. *Int. J. Mol. Sci.* **19**, 2532 (2018).
6. C. H. Heldin, A. Moustakas, Signaling receptors for TGF-β family members. *Cold Spring Harb. Perspect. Biol.* **8**, a022053 (2016).
7. M. S. Mitra, K. Lancaster, A. O. Adedeji, G. S. Palanisamy, R. A. Dave, F. Zhong, M. S. Holdren, S. J. Turley, W. C. Liang, Y. Wu, Y. G. Meng, J. M. Vernes, M. M. Schutten, A potent pan-TGFβ neutralizing monoclonal antibody elicits cardiovascular toxicity in mice and cynomolgus monkeys. *Toxicol. Sci.* **175**, 24–34 (2020).
8. M. J. Anderton, H. R. Mellor, A. Bell, C. Sadler, M. Pass, S. Powell, S. J. Steele, R. R. A. Roberts, A. Heier, Induction of heart valve lesions by small-molecule ALK5 inhibitors. *Toxicol. Pathol.* **39**, 916–924 (2011).
9. I. Gueorguieva, A. L. Cleverly, A. Stauber, N. S. Pillay, J. A. Rodon, C. P. Miles, J. M. Yingling, M. M. Lahn, Defining a therapeutic window for the novel TGF-β inhibitor LY2157299 monohydrate based on a pharmacokinetic/pharmacodynamic model. *Br. J. Clin. Pharmacol.* **77**, 796–807 (2014).
10. L. P. Sanford, I. Ormsby, A. C. G. D. Groot, H. Sariola, R. Friedman, G. P. Boivin, E. L. Cardell, T. Doetschman, TGFβ2 knockout mice have multiple developmental defects that are non-overlapping with other TGFβ knockout phenotypes. *Development* **124**, 2659–2670 (1997).
11. M. Chakrabarti, N. al-Sammarraie, M. G. Gebere, A. Bhattacharya, S. Chopra, J. Johnson, E. A. Peña, J. F. Eberth, R. E. Poelmann, A. C. Gittenberger-de Groot, M. Azhar, Transforming growth factor beta3 is required for cardiovascular development. *J. Cardiovasc. Dev. Dis.* **7**, 19 (2020).
12. Q. Du, D. Zhang, Y. Zhuang, Q. Xia, T. Wen, H. Jia, The molecular genetics of Marfan syndrome. *Int. J. Med. Sci.* **18**, 2752–2766 (2021).
13. D. Schepers, G. Tortora, H. Morisaki, G. MacCarrick, M. Lindsay, D. Liang, S. G. Mehta, J. Hague, J. Verhagen, I. van de Laar, M. Wessels, Y. Detisch, M. van Haelst, A. Baas, K. Lichtenbelt, K. Braun, D. van der Linde, J. Roos-Hesselink, G. McGillivray, J. Meester, I. Maystadt, P. Coucke, E. el-Khoury, S. Parkash, B. Diness, L. Risom, I. Scurr, Y. Hilhorst-Hofstee, T. Morisaki, J. Richer, J. Désir, M. Kempers, A. L. Rideout, G. Horne, C. Bennett, E. Rahikkala, G. Vandeweyer, M. Alaerts, A. Verstraeten, H. Dietz, L. van Laer, B. Loeys, A mutation update on the LDS-associated genes TGFB2/3 and SMAD2/3. *Hum. Mutat.* **39**, 621–634 (2018).
14. B. T. Welsh, R. Faucette, S. Bilic, C. J. Martin, T. Schürpf, D. Chen, S. Nicholls, J. Lansita, A. Kalra, Nonclinical development of SRK-181: An anti-latent TGFβ1 monoclonal antibody for the treatment of locally advanced or metastatic solid tumors. *Int. J. Toxicol.* **40**, 226–241 (2021).
15. C. J. Martin, A. Datta, C. Littlefield, A. Kalra, C. Chapron, S. Wawersik, K. B. Dagbay, C. T. Brueckner, A. Nikiforov, F. T. Danehy Jr., F. C. Streich Jr., C. Boston, A. Simpson, J. W. Jackson, S. Lin, N. Danek, R. R. Faucette, P. Raman, A. D. Capili, A. Buckler, G. J. Carven, T. Schürpf, Selective inhibition of TGFβ1 activation overcomes primary resistance to checkpoint blockade therapy by altering tumor immune landscape. *Sci. Transl. Med.* **12**, eaay8456 (2020).
16. M. A. Alikhan, M. Huynh, A. R. Kitching, J. D. Ooi, Regulatory T cells in renal disease. *Clin. Transl. Immunology.* **7**, e1004 (2018).
17. C. M. Dubois, M. H. Laprise, F. Blanchette, L. E. Gentry, R. Leduc, Processing of transforming growth factor β1 precursor by human furin convertase. *J. Biol. Chem.* **270**, 10618–10624 (1995).
18. M. Shi, J. Zhu, R. Wang, X. Chen, L. Mi, T. Walz, T. A. Springer, Latent TGF-β structure and activation. *Nature* **474**, 343–349 (2011).
19. I. B. Robertson, M. Horiguchi, L. Zilberberg, B. Dabovic, K. Hadjiolova, D. B. Rifkin, Latent TGF-β-binding proteins. *Matrix Biol.* **47**, 44–53 (2015).
20. J. Stockis, D. Colau, P. G. Coulie, S. Lucas, Membrane protein GARP is a receptor for latent TGF-β on the surface of activated human Treg. *Eur. J. Immunol.* **39**, 3315–3322 (2009).
21. Y. Qin, B. S. Garrison, W. Ma, R. Wang, A. Jiang, J. Li, M. Mistry, R. T. Bronson, D. Santoro, C. Franco, D. A. Robinton, B. Stevens, D. J. Rossi, C. Lu, T. A. Springer, A milieu molecule for TGF-β required for microglia function in the nervous system. *Cell* **174**, 156–171.e16 (2018).
22. J. Lack, J. M. O'Leary, V. Knott, X. Yuan, D. B. Rifkin, P. A. Handford, A. K. Downing, Solution structure of the third TB domain from LTBP1 provides insight into assembly of the large latent complex that sequesters latent TGF-β. *J. Mol. Biol.* **334**, 281–291 (2003).
23. S. Lienart, S. Liénart, R. Merceron, C. Vanderaa, F. Lambert, D. Colau, J. Stockis, B. van der Woning, H. De Haard, M. Saunders, P. G. Coulie, S. N. Savvides, S. Lucas, Structural basis of latent TGF-β1 presentation and activation by GARP on human regulatory T cells. *Science* **362**, 952–956 (2018).
24. Z. Duan, X. Lin, L. Wang, Q. Zhen, Y. Jiang, C. Chen, J. Yang, C. H. Lee, Y. Qin, Y. Li, B. Zhao, J. Wang, Z. Zhang, Specificity of TGF-β1 signal designated by LRRC33 and integrin $\alpha_V\beta_8$. *Nat. Commun.* **13**, 4988 (2022).
25. D. Della Ducata, J. Jaehrling, C. Hänel, M. Satzger, M. Wolber, R. Ostendorp, S. Pabst, B. Brocks, Solution equilibrium titration for high-throughput affinity estimation of unpurified antibodies and antibody fragments. *J. Biomol. Screen.* **20**, 1256–1267 (2015).
26. J. Cuende, S. Liénart, O. Dedobbeleer, B. van der Woning, G. De Boeck, J. Stockis, C. Huygens, D. Colau, J. Somja, P. Delvenne, M. Hannon, F. Baron, L. Dumoutier, J.-C. Renauld, H. De Haard, M. Saunders, P. G. Coulie, S. Lucas, Monoclonal antibodies against GARP/TGF-β1 complexes inhibit the immunosuppressive activity of human regulatory T cells in vivo. *Sci. Transl. Med.* **7**, 284ra256 (2015).
27. J. H. Tchaicha, S. B. Reyes, J. Shin, M. G. Hossain, F. F. Lang, J. H. McCarty, Glioblastoma angiogenesis and tumor cell invasiveness are differentially regulated by β8 integrin. *Cancer Res.* **71**, 6371–6381 (2011).
28. M. G. Campbell, A. Cormier, S. Ito, R. I. Seed, A. J. Bondesson, J. Lou, J. D. Marks, J. L. Baron, Y. Cheng, S. L. Nishimura, Cryo-EM reveals integrin-mediated TGF-β activation without release from latent TGF-β. *Cell* **180**, 490–501.e16 (2020).
29. J. R. Dasch, D. R. Pace, W. Waegell, D. Inenaga, L. Ellingsworth, Monoclonal antibodies recognizing transforming growth factor-beta. Bioactivity neutralization and transforming growth factor beta 2 affinity purification. *J. Immunol.* **142**, 1536–1541 (1989).
30. X. Dong, B. Zhao, R. E. Iacob, J. Zhu, A. C. Koksal, C. Lu, J. R. Engen, T. A. Springer, Force interacts with macromolecular structure in activation of TGF-β. *Nature* **542**, 55–59 (2017).
31. P. H. Weinreb, K. J. Simon, P. Rayhorn, W. J. Yang, D. R. Leone, B. M. Dolinski, B. R. Pearse, Y. Yokota, H. Kawakatsu, A. Atakilit, D. Sheppard, S. M. Violette, Function-blocking integrin $\alpha_v\beta_6$ monoclonal antibodies: Distinct ligand-mimetic and nonligand-mimetic classes. *J. Biol. Chem.* **279**, 17875–17887 (2004).
32. T. M. Chu, E. Kawinski, Plasmin, substilisin-like endoproteases, tissue plasminogen activator, and urokinase plasminogen activator are involved in activation of latent TGF-β_1 in human seminal plasma. *Biochem. Biophys. Res. Commun.* **253**, 128–134 (1998).
33. R. M. Lyons, J. Keski-Oja, H. L. Moses, Proteolytic activation of latent transforming growth factor-beta from fibroblast-conditioned medium. *J. Cell Biol.* **106**, 1659–1665 (1988).
34. H. Wei, J. Mo, L. Tao, R. J. Russell, A. A. Tymiak, G. Chen, R. E. Iacob, J. R. Engen, Hydrogen/deuterium exchange mass spectrometry for probing higher order structure of protein therapeutics: Methodology and applications. *Drug Discov. Today* **19**, 95–102 (2014).
35. M. Zhao, L. Wang, M. Wang, S. Zhou, Y. Lu, H. Cui, A. C. Racanelli, L. Zhang, T. Ye, B. Ding, B. Zhang, J. Yang, Y. Yao, Targeting fibrosis, mechanisms and cilinical trials. *Signal Transduct. Target. Ther.* **7**, 206 (2022).
36. K. Yoshioka, T. Takemura, K. Murakami, M. Okada, S. Hino, H. Miyamoto, S. Maki, Transforming growth factor-beta protein and mRNA in glomeruli in normal and diseased human kidneys. *Lab. Invest.* **68**, 154–163 (1993).
37. T. Yamamoto, N. A. Noble, A. H. Cohen, C. C. Nast, A. Hishida, L. I. Gold, W. A. Border, Expression of transforming growth factor-β isoforms in human glomerular diseases. *Kidney Int.* **49**, 461–469 (1996).
38. D. Cosgrove, D. T. Meehan, J. A. Grunkemeyer, J. M. Kornak, R. Sayers, W. J. Hunter, G. C. Samuelson, Collagen COL4A3 knockout: A mouse model for autosomal Alport syndrome. *Genes Dev.* **10**, 2981–2992 (1996).
39. J. H. Miner, J. R. Sanes, Molecular and functional defects in kidneys of mice lacking collagen alpha 3(IV): Implications for Alport syndrome. *J. Cell Biol.* **135**, 1403–1413 (1996).
40. D. Rubel, J. Boulanger, F. Craciun, E. Y. Xu, Y. Zhang, L. Phillips, M. Callahan, W. Weber, W. Song, N. Ngai, N. O. Bukanov, X. Shi, A. Hariri, H. Husson, O. Ibraghimov-Beskrovnaya, S. Liu, O. Gross, Anti-microRNA-21 therapy on Top of ACE inhibition delays renal failure in Alport syndrome mouse models. *Cells* **11**, 594 (2022).
41. V. Diwan, L. Brown, G. C. Gobe, Adenine-induced chronic kidney disease in rats. *Nephrology (Carlton)* **23**, 5–11 (2018).
42. A. Vitsky, J. Waire, R. Pawliuk, A. Bond, D. Matthews, E. LaCasse, M. L. Hawes, C. Nelson, S. Richards, P. A. Piepenhagen, R. D. Garman, L. Andrews, B. L. Thurberg, S. Lonning, S. Ledbetter, M. C. Ruzek, Homeostatic role of transforming growth factor-beta in the oral cavity and esophagus of mice and its expression by mast cells in these tissues. *Am. J. Pathol.* **174**, 2137–2149 (2009).
43. T. Sun, Z. Huang, W. C. Liang, J. Yin, W. Y. Lin, J. Wu, J. M. Vernes, J. Lutman, P. Caplazi, S. Jeet, T. Wong, M. Wong, D. J. DePianto, K. B. Morshead, K. H. Sun, Z. Modrusan, J. A. Vander Heiden, A. R. Abbas, H. Zhang, M. Xu, E. N. N'Diaye, M. Roose-Girma, P. J. Wolters, R. Yadav, S. Sukumaran, N. Ghilardi, R. Corpuz, C. Emson, Y. G. Meng, T. R. Ramalingam, P. Lupardus, H. D. Brightbill, D. Seshasayee, Y. Wu, J. R. Arron, TGFβ2 and TGFβ3 isoforms drive fibrotic disease pathogenesis. *Sci. Transl. Med.* **13**, eabe0407 (2021).
44. E. Escasany, B. Lanzón, A. García-Carrasco, A. Izquierdo-Lahuerta, L. Torres, P. Corrales, A. E. Rodríguez Rodríguez, S. Luis-Lima, C. Martínez Álvarez, F. Javier Ruperez, M. Ros, E. Porrini, M. Rydén, G. Medina-Gómez, Transforming growth factor β3 deficiency promotes defective lipid metabolism and fibrosis in murine kidney. *Dis. Model. Mech.* **14**, dmm048249 (2021).
45. Y. Zhang, P. Liu, X. Gao, W. Qian, K. Xu, rAAV2–TGF-β(3) decreases collagen synthesis and deposition in the liver of experimental hepatic fibrosis rat. *Dig. Dis. Sci.* **55**, 2821–2830 (2010).
46. Z. Chang, Y. Kishimoto, A. Hasan, N. V. Welham, TGF-β3 modulates the inflammatory environment and reduces scar formation following vocal fold mucosal injury in rats. *Dis. Model. Mech.* **7**, 83–91 (2014).

Downloaded from https://www.science.org at Dalian University of Technology on November 13, 2025

47. A. Bertrand-Chapel, C. Caligaris, T. Fenouil, C. Savary, S. Aires, S. Martel, P. Huchedé, C. Chassot, V. Chauvet, V. Cardot-Ruffino, A. P. Morel, F. Subtil, K. Mohkam, J. Y. Mabrut, L. Tonon, A. Viari, P. Cassier, V. Hervieu, M. Castets, A. Mauviel, S. Sentis, L. Bartholin, SMAD2/3 mediate oncogenic effects of TGF-β in the absence of SMAD4. *Commun. Biol.* **5**, 1068 (2022).
48. S. Mariathasan, S. J. Turley, D. Nickles, A. Castiglioni, K. Yuen, Y. Wang, E. E. KadelIII, H. Koeppen, J. L. Astarita, R. Cubas, S. Jhunjhunwala, R. Banchereau, Y. Yang, Y. Guan, C. Chalouni, J. Ziai, Y. Şenbabaoğlu, S. Santoro, D. Sheinson, J. Hung, J. M. Giltnane, A. A. Pierce, K. Mesh, S. Lianoglou, J. Riegler, R. A. D. Carano, P. Eriksson, M. Höglund, L. Somarriba, D. L. Halligan, M. S. van der Heijden, Y. Loriot, J. E. Rosenberg, L. Fong, I. Mellman, D. S. Chen, M. Green, C. Derleth, G. D. Fine, P. S. Hegde, R. Bourgon, T. Powles, TGFβ attenuates tumour response to PD-L1 blockade by contributing to exclusion of T cells. *Nature* **554**, 544–548 (2018).
49. A. Jiang, Y. Qin, T. A. Springer, Loss of LRRC33-dependent TGFβ1 activation enhances antitumor immunity and checkpoint blockade therapy. *Cancer Immunol. Res.* **10**, 453–467 (2022).
50. M. Lodyga, B. Hinz, TGF-β1 - A truly transforming growth factor in fibrosis and immunity. *Semin. Cell Dev. Biol.* **101**, 123–139 (2020).
51. R. Wang, J. Zhu, X. Dong, M. Shi, C. Lu, T. A. Springer, GARP regulates the bioavailability and activation of TGFβ. *Mol. Biol. Cell* **23**, 1129–1139 (2012).
52. D. Rifkin, N. Sachan, K. Singh, E. Sauber, G. Tellides, F. Ramirez, The role of LTBPs in TGF beta signaling. *Dev. Dyn.* **251**, 75–84 (2022).
53. J. Saharinen, J. Keski-Oja, Specific sequence motif of 8-Cys repeats of TGF-β binding proteins, LTBPs, creates a hydrophobic interaction surface for binding of small latent TGF-β. *Mol. Biol. Cell* **11**, 2691–2704 (2000).
54. M. Senior, Fighting fibrosis. *Nat. Biotechnol.* **40**, 1169–1173 (2022).
55. Y. Chang, W. L. Lau, H. Jo, K. Tsujino, L. Gewin, N. I. Reed, A. Atakilit, A. C. F. Nunes, W. F. DeGrado, D. Sheppard, Pharmacologic blockade of αvβ1 integrin ameliorates renal failure and fibrosis in vivo. *J. Am. Soc. Nephrol.* **28**, 1998–2005 (2017).
56. M. L. Decaris, J. R. Schaub, C. Chen, J. Cha, G. G. Lee, M. Rexhepaj, S. S. Ho, V. Rao, M. M. Marlow, P. Kotak, E. H. Budi, L. Hooi, J. Wu, M. Fridlib, S. P. Martin, S. Huang, M. Chen, M. Muñoz, T. F. Hom, P. J. Wolters, T. J. Desai, F. Rock, K. Leftheris, D. J. Morgans, E. I. Lepist, P. Andre, E. A. Lefebvre, S. M. Turner, Dual inhibition of $\alpha_v\beta_6$ and $\alpha_v\beta_1$ reduces fibrogenesis in lung tissue explants from patients with IPF. *Respir. Res.* **22**, 265 (2021).
57. A. E. John, R. H. Graves, K. T. Pun, G. Vitulli, E. J. Forty, P. F. Mercer, J. L. Morrell, J. W. Barrett, R. F. Rogers, M. Hafeji, L. I. Bibby, E. Gower, V. S. Morrison, Y. Man, J. A. Roper, J. C. Luckett, L. A. Borthwick, B. S. Barksby, R. A. Burgoyne, R. Barnes, J. le, D. J. Flint, S. Pyne, A. Habgood, L. A. Organ, C. Joseph, R. C. Edwards-Pritchard, T. M. Maher, A. J. Fisher, N. S. Gudmann, D. J. Leeming, R. C. Chambers, P. T. Lukey, R. P. Marshall, S. J. F. Macdonald, R. G. Jenkins, R. J. Slack, Translational pharmacology of an inhaled small molecule αvβ6 integrin inhibitor for idiopathic pulmonary fibrosis. *Nat. Commun.* **11**, 4659 (2020).
58. V. Q. Le, B. Zhao, S. Ramesh, C. Toohey, A. DeCosta, J. Mintseris, X. Liu, S. Gygi, T. A. Springer, A specialized integrin-binding motif enables proTGF-β2 activation by integrin αVβ6 but not αVβ8. *Proc. Natl. Acad. Sci. U.S.A.* **120**, e2304874120 (2023).
59. J. P. Annes, D. B. Rifkin, J. S. Munger, The integrin $\alpha_V\beta_6$ binds and activates latent TGFβ3. *FEBS Lett.* **511**, 65–68 (2002).
60. M. Guffroy, B. Trela, T. Kambara, L. Stawski, H. Chen, L. Luus, M. S. Montesinos, L. Olson, Y. He, K. Maisonave, T. Carr, M. Lu, A. S. Ray, L. A. Hazelwood, Selective inhibition of integrin αvβ6 leads to rapid induction of urinary bladder tumors in cynomolgus macaques. *Toxicol. Sci.* **191**, 400–413 (2023).
61. G. Raghu, M. Mouded, D. C. Chambers, F. J. Martinez, L. Richeldi, L. H. Lancaster, M. J. Hamblin, K. F. Gibson, I. O. Rosas, A. Prasse, G. Zhao, M. Serenko, N. Novikov, A. McCurley, P. Bansal, C. Stebbins, M. Arefayene, S. Ibebunjo, S. M. Violette, D. Gallagher, J. Behr, A phase IIb randomized clinical study of an anti-$\alpha_v\beta_6$ monoclonal antibody in idiopathic pulmonary fibrosis. *Am. J. Respir. Crit. Care Med.* **206**, 1128–1139 (2022).
62. Z. Zou, P. D. Sun, Overexpression of human transforming growth factor-β1 using a recombinant CHO cell expression system. *Protein Expr. Purif.* **37**, 265–272 (2004).
63. M. Hara, I. Inoue, Y. Yamazaki, A. Kirita, T. Matsuura, S. L. Friedman, D. B. Rifkin, S. Kojima, L59 TGF-β LAP degradation products serve as a promising blood biomarker for liver fibrogenesis in mice. *Fibrogen. Tiss. Rep.* **8**, 17 (2015).
64. W. Kabsch, XDS. *Acta Crystallogr. D Biol. Crystallogr.* **66**, 125–132 (2010).
65. A. J. McCoy, R. W. Grosse-Kunstleve, P. D. Adams, M. D. Winn, L. C. Storoni, R. J. Read, Phaser crystallographic software. *J. Appl. Cryst.* **40**, 658–674 (2007).
66. P. Emsley, K. Cowtan, Coot: Model-building tools for molecular graphics. *Acta Crystallogr. D Biol. Crystallogr.* **60**, 2126–2132 (2004).
67. G. N. Murshudov, P. Skubák, A. A. Lebedev, N. S. Pannu, R. A. Steiner, R. A. Nicholls, M. D. Winn, F. Long, A. A. Vagin, REFMAC5 for the refinement of macromolecular crystal structures. *Acta Crystallogr. D Biol. Crystallogr.* **67**, 355–367 (2011).
68. T. E. Wales, K. E. Fadgen, G. C. Gerhardt, J. R. Engen, High-speed and high-resolution UPLC separation at zero degrees celsius. *Anal. Chem.* **80**, 6815–6820 (2008).
69. S. J. Geromanos, J. P. C. Vissers, J. C. Silva, C. A. Dorschel, G. Z. Li, M. V. Gorenstein, R. H. Bateman, J. I. Langridge, The detection, correlation, and comparison of peptide precursor and product ions from data independent LC-MS with data dependant LC-MS/MS. *Proteomics* **9**, 1683–1695 (2009).
70. T. E. Wales, J. R. Engen, Hydrogen exchange mass spectrometry for the analysis of protein dynamics. *Mass Spectrom. Rev.* **25**, 158–170 (2006).
71. D. Houde, S. A. Berkowitz, J. R. Engen, The utility of hydrogen/deuterium exchange mass spectrometry in biopharmaceutical comparability studies. *J. Pharm. Sci.* **100**, 2071–2086 (2011).
72. F. Madeira, M. Pearce, A. R. N. Tivey, P. Basutkar, J. Lee, O. Edbali, N. Madhusoodanan, A. Kolesnikov, R. Lopez, Search and sequence analysis tools services from EMBL-EBI in 2022. *Nucleic Acids Res.* **50**, W276–W279 (2022).

Acknowledgments: We acknowledge T. A. Springer (Harvard Medical School) for the foundational structural biochemistry that enabled the targeting of latent complexes of TGF-β1 and N. Mahanthappa (founder and former CEO of Scholar Rock) for strategic and organizational contributions to the work described herein. We acknowledge A. Polzin, L. Cortes, and M. Alsuraih of Scholar Rock for reading and editing this manuscript. We thank the antibody discovery team at Adimab in Lebanon, NH, for contributions to the discovery of LTBP-49247. We thank S. Ramachandran and A. Wolfe of Ichor Lifesciences Inc. for efforts in obtaining the x-ray crystal structures presented here. We thank S. J. Eyles of the UMass Institute of Applied Life Sciences Mass Spectrometry core facility for assistance with H/DX-MS data collection. We thank L. Liu and M. Fulham of Scholar Rock for independent statistical review of the methods used to analyze rodent pharmacology studies. **Funding:** This study was funded by Scholar Rock Inc. **Author contributions:** A.I.F., J.W.J., F.C.S., R.M., and A.P. wrote the original draft of the manuscript. A.I.F., J.W.J., F.C.S., and A.P. assembled the figures and tables; J.W.J., F.C.S., A.I.F., G.C., A.P., S.B.N., S.W., T.S., G.J.C., A.B., M.Q., and A.D. designed the experiments and contributed the additional edits; S.W., T.S., M.Q., and A.B. had the overall study responsibility and directed the research. G.C., A.I.F., and C.C. conducted the in vivo pharmacology studies in Alport and rat adenine models; A.P. and M.W. conducted and analyzed the toxicology studies in mice. M.K. and S.C. performed the studies to measure concentration of antibodies in serum for toxicokinetic and pharmacology studies. C.B., F.C.S., F.T.D., and S.B.N. purified and characterized the protein used throughout the study. C.L. and C.C. conducted in vitro analysis in integrin- and kallikrein-mediated TGF-β activation assays. S.L. designed and conducted the MSD-SET experiments. J.W.J. designed and conducted the MSD-SET, Biacore, and Octet experiments. C.J.M. and G.C. performed T_{reg} binding assays. C.T.B. and K.L. conducted the histological analysis (PSR and pSMAD2) on kidney tissue. A.Z. conducted multiplexed fluorescent analysis of pSMAD2 in cell populations in kidney tissue. S.K., A.D., and J.W.J. directed and performed the antibody discovery work to identify LTBP-49247. K.C. and C.C. performed the quantitative polymerase chain reaction analysis from tissue samples. K.B.D. performed the H/DX studies. F.C.S., S.B.N., and C.B. conducted the crystallography and structural analysis of the LTBP-49247/TGF-β1 complex. **Competing interests:** All authors were Scholar Rock employees at the time of the work described herein and stock and/or stock option holders, except for M.W., who was a consultant and received consulting fees from Scholar Rock. M.Q. is the chief scientific officer at Scholar Rock Inc. G.J.C. and A.B. are former chief scientific officers of Scholar Rock Inc. J.W.J., F.C.S., G.C., C.L., S.W., A.D., T.S., and A.I.F. are named inventors on an international patent application related to this work (published as WO/2020/160291; LTBP complex–specific inhibitors of TGF-β and uses thereof) filed by Scholar Rock Inc. J.W.J., G.C., and T.S. are inventors on a related international patent application (published as WO/2023/288277; LTBP complex–specific inhibitors of TGF-β1 and uses thereof). **Data and materials availability:** The sequences of LTBP-49247 have been published in the above-referenced patent applications, and the sequences of TGFb1-37021 have been published in patent application WO/2021/142427; TGF-β inhibitors and use thereof. The coordinates of the TGF-β1:LTBP-49247 Fab complex crystal structure have been deposited at the PDB with the accession number 8UDZ. All other materials required to evaluate the conclusions in the paper are described in the paper or the Supplementary Materials. Antibodies or sequences may be provided by Scholar Rock under a material transfer agreement.

Submitted 8 January 2024
Accepted 11 June 2024
Published 9 July 2024
10.1126/scisignal.adn6052

Downloaded from https://www.science.org at Dalian University of Technology on November 13, 2025